Is waste heat recovery a promising avenue for the Carnot battery? Techno-economic optimisation of an electric booster-assisted Carnot battery integrated into different data centres

Antoine Laterre[a,b,*], Olivier Dumont[b], Vincent Lemort[b], Francesco Contino[a]

[a] *Institute of Mechanics, Materials and Civil Engineering (iMMC), Université catholique de Louvain (UCLouvain), Place du Levant, 2, Louvain-la-Neuve, 1348, Belgium*
[b] *Thermodynamics Laboratory, University of Liège (ULiège), Allée de la Découverte 17, Liège, 4000, Belgium*

Abstract

The transition to intermittent renewable energies will necessitate the integration of storage. An interesting technology is the Carnot battery (CB), a novel power-to-heat-to-power system, capable of harnessing waste energy streams. While initial studies have indicated that, under ideal conditions, CB can be competitive with conventional technologies such as chemical batteries, their economic viability in real-world applications remains uncertain. To fill this gap, this work explores the techno-economic potential of electric booster-assisted CB integrated within data centers. Motivation for this case study is the recovery of waste heat, leading to an improved electrical storage efficiency. To maximise the energy self-sufficiency and the internal rate of return, we have applied multi-criteria optimisation to the system design, under three different thermal integration scenarios and for two sets of climatic conditions, using a thermodynamic model and time series from a real data centre. Our analyses suggest that current projections for electricity prices and CB costs yield payback periods exceeding a decade, but that these could fall below ten years if the CB capital costs were halved. Furthermore, it turns out that the choice of optimum charging system (i.e. right balance between heat pump and electrical heater) is contingent on the heat source temperature and availability. For higher temperatures (e.g. 60°C), heat pumps emerge as the financially

*Corresponding author.
Email address: `antoine.laterre@uclouvain.com` (Antoine Laterre)

most attractive option, thanks to their superior coefficient of performance, whereas for lower temperatures ($<$ 25°C), resistive heaters are preferable. Results also show that when the aim is to increase the energy self-sufficiency, there exist an efficiency/charging capacity trade-off, which causes a dilemma for the system design. On the one hand, heat pumps are vital to increase the efficiency of the CB, but on the other hand, as the amount of thermal energy available at its source is limited by the data centre operations, electrical boosters are indispensable to increase the charging capacity. To soften this dilemma and enhance the techno-economic performance of thermally integrated CB, future research should explore more efficient booster configurations, such as dual heat source heat pumps.

Keywords:

Carnot Battery, Thermally Integrated Pumped Thermal Energy Storage (TI-PTES), Waste Heat Recovery, Data Centre, Techno-Economic Analysis, Multi-Criteria Optimisation

---

1. Introduction

Energy storage is recognised as a key driver in the transition to intermittent and non-dispatchable renewable energy sources (e.g. wind, solar), as it contributes to bridge the gap between production and demand [1]. In this context, finding cost-effective storage systems has become essential. At the same time, in order to limit the costly production and storage capacity that needs to be installed, it has become necessary to increase the flexibility and the efficiency of energy systems. This involves supporting sector coupling and recovering lost energy flows (e.g. waste heat, curtailment), so as not to lose any of this precious energy [2]. From this perspective, Carnot batteries (CB), which bring together various power-to-heat-to-power concepts, turn out to be promising devices. Indeed, these multi-energy flexibility options combine energy storage, coupling to thermal systems and waste heat recovery [3–5].

1.1. Techno-economic analyses of Carnot batteries

Carnot batteries store energy under the form of heat in thermal energy storage (TES) systems. In most implementations, these TES are charged with high temperature heat

Nomenclature

Greek and Latin symbols

Δp	pressure losses, bar
ΔT	temperature difference, K
η	efficiency, %
ρ	energy density, kWh/m³
τ	time, h
B_n	benefits at year n, €$_{2021}$
C_0	capital cost, €$_{2021}$
C_n	costs at year n, €$_{2021}$
E	energy, kWh
G	solar irradiance, W/m²
LT	lifetime, year
P	power, kW
p	pressure, bar
r	discount rate, %
T	temperature, °C
V	volume, m³

Sub- and superscripts

ch	charge
disch	discharge

Symbols

CF	capacity factor
CAPEX	capital expenditures
CB	Carnot battery
COP	coefficient of performance
DPP	discounted payback-period
HE	heat engine
HP	heat pump
IRR	internal rate of return
KPI	key performance indicator
LCOS	levelised cost of storage
NPV	net present value
ORC	organic Rankine cycle
PV	photovoltaic
RH	resistive heater
SSR	self-sufficiency ratio
TES	thermal energy storage
TI-PTES	thermally integrated pumped thermal energy storage
WHR	waste heat recovery

pumps (HP), including mechanical vapor compression and inverse closed Brayton cycles. To a lesser extent, they can be charged with resistive heaters. They are then discharged with heat engines (HE) that produce electricity [6]. Most HE technologies are either based on the closed Brayton cycle, or on the (organic) Rankine cycle (ORC) [6]. An interesting feature of CB is the possible coupling with thermal flows at low or high temperature, making them strong flexibility options for sector coupling [7]. Other advantages are the low expected investment costs and environmental footprint [6]. Indeed, most concepts propose to store heat in cheap and abundant materials, such as rock and water [6, 8]. A typical architecture for Rankine based CB is depicted in Fig. 1.

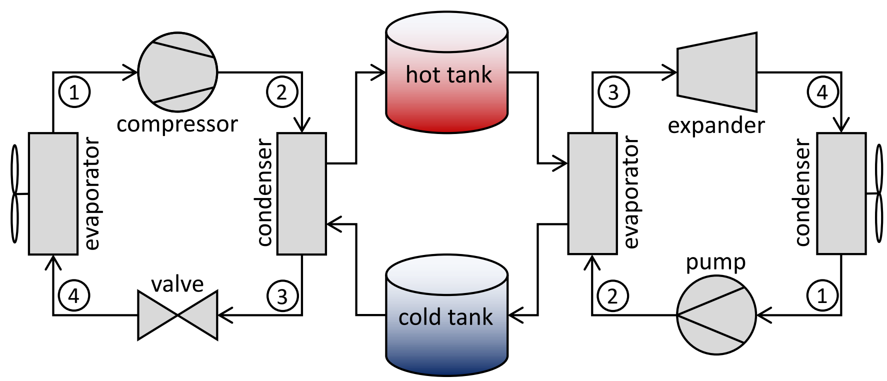

Figure 1: Architecture of a basic Carnot battery based on vapor compression heat pump (left), two-tanks sensible heat thermal storage (centre) and organic Rankine cycle (right). Note that here, the HP and the ORC are air-sourced and air-cooled.

Carnot batteries for low temperature thermal coupling (i.e. < 100°C) are generally referred to as thermally integrated pumped thermal energy storage (TI-PTES) [4]. In these systems, the heat source used at the HP evaporator can have different origins. They include geothermal sources, heating networks, seasonal TES, solar thermal, etc. [9]. Another particularly interesting option is the recovery of low-grade waste heat (e.g. data centre cooling, sewage treatment, etc.), which increases the overall efficiency of the energy system.

Since the introduction of the basic architecture (depicted in Fig. 1) in 2017 by Frate *et al.* [4], several improvements have been investigated for TI-PTES. Dumont and Lemort [10] and Staub *et al.* [11] have characterised the technical performance of a reversible HP/ORC system so as to reduce the capital cost of the CB. In 2020, Frate *et al.* [12] showed that the use internal regeneration in the HP and in the ORC increases the exergy efficiency by up to 15%, and that it had the potential of being established as the reference configuration for the CB. Weitzer *et al.* [5, 13] looked in 2022 at the potential of using organic flash cycles for the discharge so as to simultaneously increase the energy density without degrading the discharge efficiency, by providing a better thermal match between a sensible TES and the cycle. They concluded that only advanced cycles relying on wet expansion could bring performance improvements, despite the additional complexity. Weitzer *et al.* [13] also introduced the Carnot battery trilemma, which reflects the conflict between power-to-power efficiency, exergy efficiency and electrical energy energy density in TI-PTES. The same year, Lu *et al.* [14] studied the benefit of using zeotropic cycles, whose potential in TI-PTES with sensible TES had already been mentioned several times in the literature, but never studied [11, 13]. They showed that, under optimised conditions, the roundtrip efficiency could be increased by more than 20%. More recently, Zhang *et al.* [15] introduced a new TI-PTES architecture able to recover waste heat both during the charge and the discharge. Roundtrip efficiency gains of more than 10% were reached.

However, although these studies have shown that there are a multitude of possible designs and thermal integration scenarios, they do not yet indicate exactly where and how CB could become relevant and cost-effective for energy systems [7, 8, 16]. For example, it is not yet clear what services they should provide in the various scenarios: Pure load shifting? Energy arbitrage? Grid services? Electrical and/or thermal discharge? Storage duration? etc. [7, 16, 17]. Nor is it clear at what cost and efficiency they might begin to penetrate the market. In other words, it has not yet been determined precisely which designs would enable CB to be technically and financially sound in the different scenarios.

To answer these questions, some studies have recently sought to compare and optimise the techno-economic performance of different machines, assuming cyclic and ideal boundary conditions (e.g. constant efficiencies and power profiles over time, fixed number of charge and discharge cycles over lifetime, etc.). For example, Hu *et al.* [18] optimised the levelised cost of storage (LCOS) and roundtrip efficiency (η_{cb}) of the basic TI-PTES for different heat source temperatures. They obtained a LCOS of 300 \$/MWh and η_{cb} of 70% when the heat source temperature was 85°C. They also proved that the LCOS and η_{cb} were strictly conflicting in all cases, showing that the HP evaporation temperature and storage temperature levels were key variables to arbitrate the trade-off. For a source temperature of 80°C and considering regenerated and non-regenerated cycles for charge and discharge, Fan and Xi [19] obtained worse performance, with a LCOS of about 420 \$/MWh, corresponding on average to $\eta_{\text{cb}} =$ 25%. They also showed that these two objectives were strictly conflicting. Okten and Kursun [20] looked at a hybrid CB coupled with an absorption refrigeration system and with a source at 90°C. They obtained a LCOS of 242 \$/MWh. For a source at 80°C and considering regenerated and non-regenerated cycles, Zhang *et al.* [21] reported an average efficiency of 20%, corresponding to a LCOS of around 300 \$/MWh. These values are similar to those reported by [19]; however, such η_{cb} is well below the values usually encountered in the literature [4, 5, 12]. Finally, Frate *et al.* [22] also showed that the specific cost of the CB was in conflict with η_{cb}.

Generally speaking, these studies concluded that thermally integrated Carnot batteries could be competitive with chemical batteries. However, the ideal conditions in which they were studied probably made the results too optimistic. In practice, the conditions under which they would operate would be less ideal. Due to intermittent operations, charge and discharge times could vary. Similarly, power profiles could fluctuate in frequency and amplitude over time. Also, the temperatures at the boundaries of the thermal machines will probably not be constant (e.g. ambient), which affects their efficiency. Finally, the link between power levels and heat source availability could be a real operating constraint, limiting the charging capacity.

To address these shortcomings, new studies have produced scenario based analyses. In these, time series representing different integration scenarios are used to simulate the system behaviour on an hour-by-hour basis. Frate *et al.* [17] studied the potential of TI-PTES for multi-energy districts. Through a mixed integer linear model, they conducted optimal power flow analyses on a fixed TI-PTES design. Considering higher capital costs than in the above cited studies, they showed that the total annualized cost was around double compared to chemical battery storage, and that TI-PTES could not achieve financial feasibility.

Sorknæs *et al.* [23] investigated the economic potential of large-scale integration of CB in 100% renewable energy systems. In this macro analysis, they used the EnergyPLAN model [24] in the case of Denmark to assess the economic viability of different CB concepts, and to identify a target LCOS leading to financial feasibility. They showed that currently existing stand-alone CB concepts (i.e. without thermal integration) are not able to achieve economic feasibility today, and that solutions for cost reductions are therefore required. Yet, they showed that if a LCOS of about 60 €/MWh is reached, CB can be used to reduce the need for renewable fuels.

Tassenoy *et al.* [25] looked at the use of CB for photovoltaic (PV) load shifting in an office building. With a constant efficiency model, they used synthetic production and consumption profiles to optimise the net present value (NPV) of a CB that recovers the 50°C waste heat from a data centre. They showed that, using the day ahead electricity prices of 2019 and without subsidy or tax mechanisms, it was not possible to obtain positive NPV. They also showed that the CB could become competitive with Li-ion batteries when charging and discharging times exceeded 7 hours.

Poletto *et al.* [26] were also interested in the integration of CB in a data centre powered in part by PV. In particular, they considered the beneficial effect of the simultaneous production of heating and cooling by the heat pump, which reduces the consumption of the data centre cooling units. They showed that for high spot electricity prices (i.e. those of the 2022 energy crisis) and moderate investment costs, the NPV could be positive (i.e. discounted payback period less than 15 years).

The difference between the conclusions of Tassenoy *et al.* and Poletto *et al.* is essentially due to the fact that Tassenoy *et al.* considered higher investment costs while using lower electricity prices. Poletto *et al.* also carried out a study using the 2018 electricity prices and came to the same conclusion as Tassenoy *et al.*: it is not possible to have a positive NPV with low electricity prices (i.e. discounted payback period is always longer than lifetime). Another result shared by Tassenoy *et al.* and Poletto *et al.* is that, for a given case study, the greater the CB storage capacity, the longer the payback. Tassenoy *et al.* even showed that the NPV is lower for larger capacities. This is in contrast to the previously cited studies, which generally recommend increasing capacity to benefit from scale effects.

1.2. Aims of this study and work novelty

In the above mentioned studies, when techno-economic optimisation was carried out, the models generally assumed fixed efficiencies over the operations and did not take into account the constraint on the availability of the heat source (i.e. they assumed infinite source). When more advanced models taking into account variations in efficiency were considered, no optimisation of the installed capacity and power was carried out. At best, in the case of Poletto *et al.*, a parametric analysis of the TES tank volumes was carried out. It should also be noted that, with the exception of McTigue *et al.* [27] who studied Brayton based CB, hardly any study has taken into account the impact of techno-economic uncertainties on the results obtained. Finally, none of the above studies exploited the synergies between renewable generation and storage capacity: fixed PV capacity was always assumed.

In order to properly consider operational constraints (e.g. variation in efficiencies, availability of the heat source) while seeking to achieve better financial performance, this work proposes to simultaneously optimise the design of a CB (i.e. capacity and thermodynamic cycle) and of a PV system in a real 100 kW data centre. This is achieved using an accurate model of the system. The case of the data centre is of interest for the Carnot battery because few other technologies are able to recover its waste heat. Indeed, ORC have poor efficiency due to low temperatures [28] and direct heat reuse cannot really be envisaged because there is rarely a local need for heat throughout the year (e.g. summer).

One specific feature of the CB concept studied here is the optional use of a resistive heater (RH) to charge the system. Although it is less efficient, it reduces the investment costs and reduces the dependency on the heat source availability.

This paper first presents the different investigated scenarios with the associated annual time series. It then introduces the model of the PV + CB system, along with a description of the power management strategy. After that, it describes the economic model used to quantify financial performance. It then presents the optimisation problem. In addition, a series of technical and operational uncertainties are taken into account to analyse the sensitivity of the results, thanks to an effective propagation method. The results of the multi-criteria analysis are then discussed. This is followed by a detailed analysis of certain designs offering good technical performance. Finally, a conclusion summarises the results obtained in this study and highlights some future research directions.

2. Model and methods

The objective of this work is to assess the techno-economic performance of a PV system and a CB integrated in a data centre. Different case studies are compared by optimising the design of the PV + CB system, in order to maximise the data centre energy self-sufficiency while maximising the financial performance of the investment. The different case studies, models and optimisation criteria are introduced below.

2.1. Case studies

The layout of the studied energy system is shown in Fig. 2 to illustrate how the PV and CB are integrated into the data center. Three scenarios are investigated to compare the performance of some possible integration schemes for the CB, depending on the type of data centre cooling system. In short, these are distinguished by the temperature and availability of the heat source. In practice, the two main categories of data centres (i.e. indirectly and directly cooled) are here considered. According to the power of the data centre, different configurations and technologies can be used, as each offers its own advantages (cost, efficiency, complexity, etc.). Nevertheless, in order to limit the number of cases to be dealt with, only those offering the best energy performance and being the most widespread are dealt with in this study.

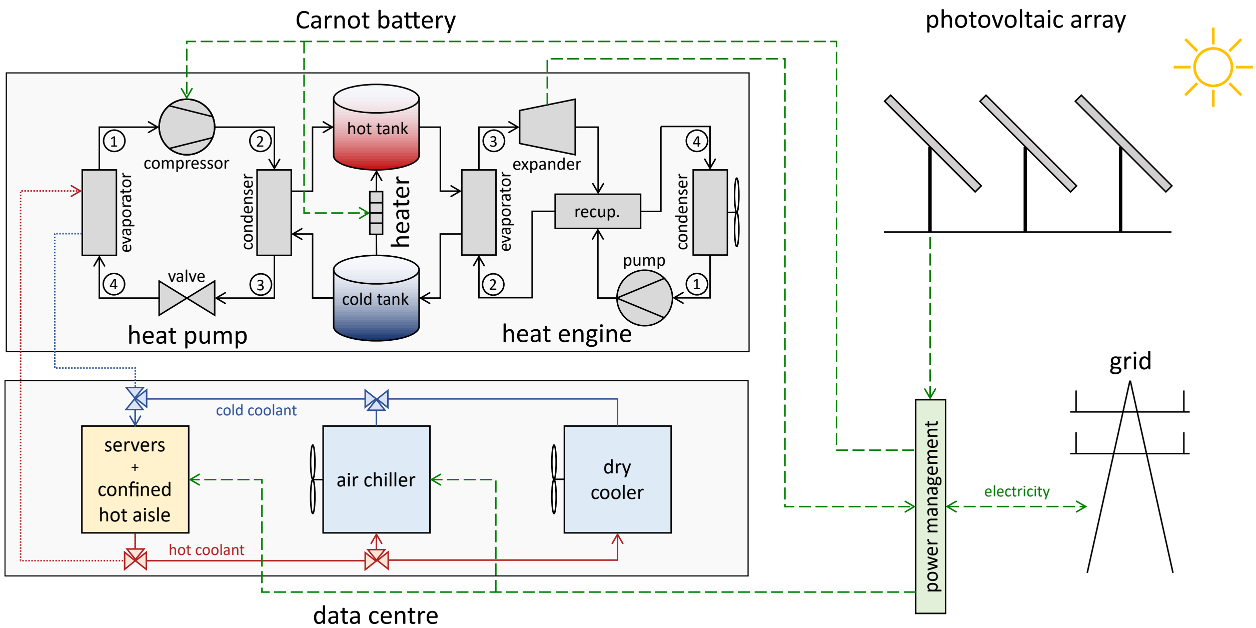

Figure 2: Layout of the Carnot battery and photovoltaic system integrated into the data center. In scenarios A and B, a new connection is made between the cooling circuit and the heat pump evaporator (dotted lines). In scenario B, the coolant directly flows through the servers (i.e. direct cooling), so the confined aisle is unused. In scenario C, the heat pump uses an aero-evaporator (i.e. no connection with the cooling circuit, fan not represented here). Note that the components necessary for the control of the CB are not depicted here (e.g. liquid receiver, ...).

Aside from the type of data centre, two locations are used to take into account different climatic conditions, which affect the system performance (e.g. PV production, CB efficiency, etc.): Louvain-la-Neuve (Belgium), with a temperate climate and moderate solar irradiance, and Seville (Spain), with a hot climate and higher irradiance (see Fig. 3 for ambient temperatures and solar irradiances). These different case studies are summarised in Table 1.

In all scenarios, the data centre, which consumes electricity to power the servers and the cooling system, can be powered either by the PV system, the CB or the distribution grid. When the PV system is overproducing compared with demand, electricity can either be used to charge the CB or be returned to the grid at a zero feed-in tariff (i.e. which is equivalent to

Location	**Louvain-la-Neuve**			**Seville**		
Scenario	**A**	**B**	**C**	**A**	**B**	**C**
Coolant temperature [°C]	24	60	24	24	60	24
Servers consumption [MWh]	895.9	895.9	895.9	895.9	895.9	895.9
Chiller consumption [MWh]	69.1	0.0	69.1	147.2	0.0	147.2
Heat source of heat pump	coolant	coolant	ambient	coolant	coolant	ambient
Average ambient temp. [°C]	10.8	10.8	10.8	18.5	18.5	18.5
Average solar irrad. [W/m²]	150.6	150.6	150.6	228.5	228.6	228.6

Table 1: Summary of the investigated integration scenarios for the Carnot battery in data centres. The energy consumption are assessed on an annual basis using the time series from the UCLouvain data centre. The solar irradiance and ambient temperature correspond to average values for 2019.

curtailment in an economic perspective). In this sense, load-shifting of the PV production is the only service that the CB can provide to the system. The reasons for these choices and the detailed power management strategy are introduced below.

2.1.1. Scenario A: air-cooled data centres (indirect cooling)

Today, most low-power data centres (i.e. < 1 MW) are cooled indirectly with air. Several configurations exist, but one of the most efficient uses hot aisles, so that is the one we have chosen for this scenario. Fresh ambient room air (i.e. generally below 25°C) is supplied to the servers racks to cool them. Once it has warmed up, it is collected at the racks outlet and pulsed with small fans in a hot aisle. In this aisle, the hot air is confined beneath a plastic cover so as not to heat up the rest of the room by mixing with the surrounding air. It is then drawn in liquid cooling packages where it transfers its heat to chilled water (i.e. generally $<$ 15°C) before being discharged into the room. Chilled water is typically produced in two different ways, depending on the outside temperature. When this temperature is below a given threshold (usually around 10°C), the hot water from the liquid cooling packages is cooled directly by the external air in a dry cooler. When the outside temperature is above this threshold, an air chiller takes over, resulting in an additional electricity consumption.

This combination of cooling systems is illustrated in Fig. 2.

In this integration scenario, the heat pump of the CB uses the cooling water as a heat source. This increases its coefficient of performance (COP) and reduces the chiller's electricity consumption, as less water needs to be cooled down by it. However, as the amount of thermal energy available at the HP evaporator is limited by the servers operations, a booster can be used in parallel (i.e. the RH in this scenario). In other respects, although its equivalent COP is only 1, this RH is much cheaper than an HP (almost three times less for the same thermal power, as shown in the economic model in Section 2.3), which could make it more attractive from a techno-economic point of view. More complex combinations, for example with an HP that would use outside air as a second source, are not considered here but will form part of a future study. An HP using only outside air is covered by scenario C.

In order to evaluate its performance, the system is simulated with an hourly resolution using an accurate thermodynamic model and time series from a real data centre, following a rule-based power management strategy. These are presented in Section 2.2. These time series, corresponding to the year 2021, have been gratefully provided by the *Center for High Performance Computing and Mass Storage* from UCLouvain and are illustrated in Fig. 3. The data centre was commissioned in 2016 and has an installed capacity of about 100 kW. Its hot cooling water temperature is 24°C and the chilled water is produced at 14°C. The ambient temperature threshold for switching between the dry cooler and the chiller is 12°C. The ambient temperature and solar irradiance in Fig. 3 have been obtained with `Renewables.ninja` [29, 30] and correspond to the year 2019. Please note that the consumption data for the chiller was not available, so it has been artificially synthesised assuming a fixed second law efficiency, such as described in Section 2.2.3.

2.1.2. Scenario B: liquid-cooled data centres (direct cooling)

A new generation of servers is currently being developed to provide higher power densities, limit the energy consumption of cooling units, and reject a higher temperature heat, so that it could be better recycled. In this new generation, the servers are cooled directly with

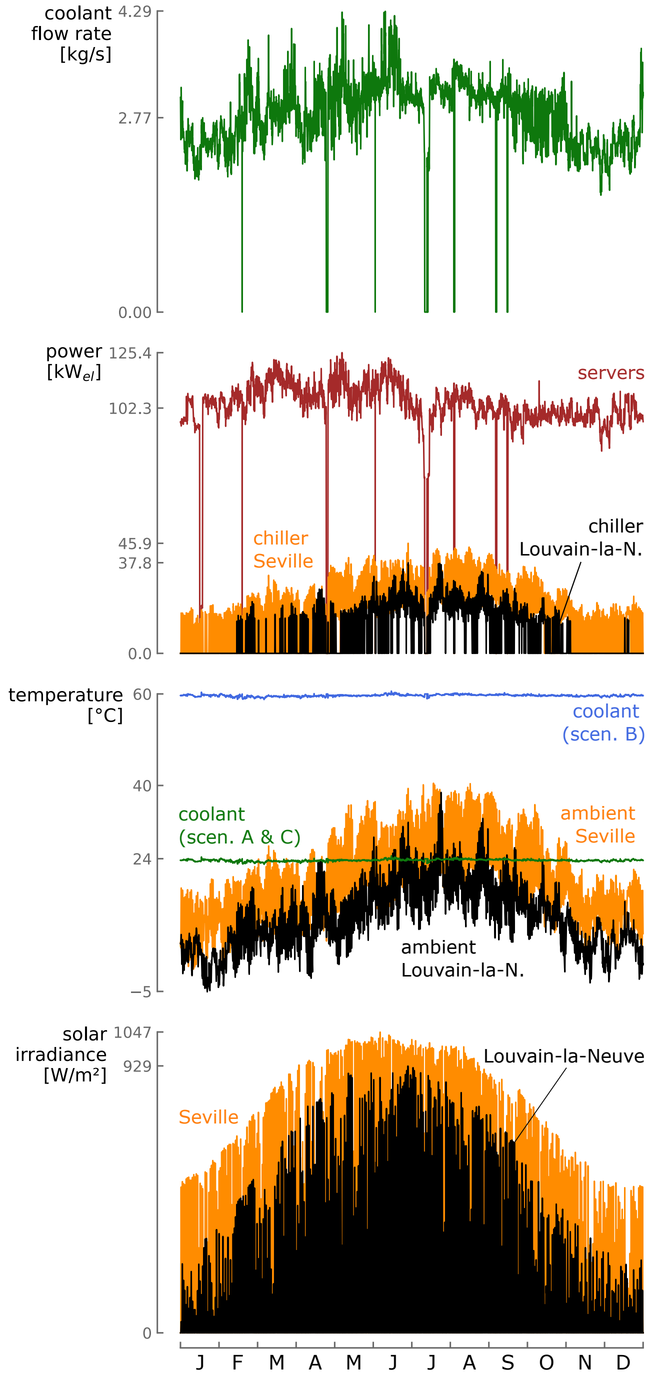

Figure 3: The hourly solar irradiance, ambient and coolant temperatures, electrical power demand (servers and chiller) and coolant flow rates profiles for Louvain-la-Neuve and Seville. They show that the chillers consumption increases during spring and summer and decreases during fall and winter.

the liquid coolant that circulates in them. This enables much higher coolant temperatures to be reached, ranging from 50°C up to 75°C (most servers have an operating temperature limited to 80°C) [28]. As these temperatures are systematically higher than the ambient temperature, the cooling unit can operate using dry cooling only. In this work, a conservative value of 60°C was selected to model the cooling water, as shown in Fig. 3.

From the CB point of view, the benefit of this scenario is that the heat source is at a higher temperature, what significantly increases the COP of the HP, and a fortiori η_{cb}. However, as the amount of waste heat remains constrained by the servers operations, the electrical booster can still be used in complement to the HP to charge the storage.

2.1.3. Scenario C: standalone air-sourced Carnot battery

In scenarios A and B, a thermal booster can be used to overcome the constraint on the availability of the heat source. Also, its much lower cost puts it in competition with the more expensive HP. However, its utilisation results in a lower equivalent charging COP for the CB, and a techno-economic trade-off therefore needs to be found.

As an alternative to overcome the constraint on the availability of the heat source, scenario C uses a non-integrated CB, where the source of the HP is the ambient. The resulting heat pump COP is lower than in scenarios A and B (especially in Louvain-la-Neuve where the ambient temperature is lower). However, as there is no longer any constraint on the heat source, the electric booster is no longer essential to increase charging capacity, enabling potentially higher equivalent charging COP. Nevertheless, the booster and the HP remain in competition from an economic point of view, thus the use of a RH remains an option in this scenario.

Table 1 summarises and compares the technical performance of the different scenarios when no PV and no CB is installed (i.e. the current case), based on data from the UCLouvain data centre and for the cases of Louvain-la-Neuve and Seville.

2.2. Detailed description and physical modelling of the system

2.2.1. Carnot battery

As depicted in Fig. 2, the CB under investigation is composed of a single-stage high-temperature heat pump, a resistive heater that is used as a thermal booster (i.e. additional charging capacity when the HP runs at nominal load), a two-tanks sensible heat thermal energy storage and an air-cooled recuperated organic Rankine cycle. The working fluid used in the HP and in the ORC is R1233zd(E), as it has shown interesting performance and behaviour in other Carnot batteries with similar working conditions [10, 12].

The performance and operating conditions (i.e. physical and energy flows) of the thermal machines are assessed by evaluating their thermodynamic cycle and applying energy balances at each hour the year for the prescribed boundary conditions. This is done with an in-house `Python` model and based on the quasi-steady state assumption (i.e. steady-sate operation at each hour, no transient considered). The values of the parameters used in this model are given in Table 2. The temperature levels within the thermal machines are obtained for the given boundary conditions (i.e. temperatures of the heat source, thermal storage and ambient air) using a constant pinch-point model [31]. The thermodynamic properties of the fluids are assessed using `CoolProp` [32]. The resistive heater is modelled with a black-box approach, assuming 100% efficiency and full load flexibility, without efficiency degradation.

In practical applications, more advanced cycles than those shown in Fig. 2, such as two-stage or cascaded heat pumps, should certainly be investigated for performance and technical reasons (e.g. high pressure ratios). Nevertheless, the main purpose of the present model is only to obtain physical and energy flows during charging and discharging operations, necessary to carry out the techno-economic analysis. To this end, and at this stage of the investigation of the case study, modelling the charging and discharging systems using basic cycles seems sufficient. If the results show interesting performance, more advanced systems could be studied in future works.

Parameter	Symbol	Value	Units	Ref./Reason
Compressor isentropic efficiency	$\eta_{\text{is,comp}}$	0.65	-	*see Section 2.2.1*
Pressure losses in HP	Δp_{hp}	0	bar	[12, 13]
Heat source temperature glide	$\Delta T_{\text{hs,gl}}$	10	K	*see Section 2.1*
HP vapor superheat	$\Delta T_{\text{hp,sh}}$	3	K	[13]
HP liquid subcooling	$\Delta T_{\text{hp,sc}}$	max.	K	[33]
Pinch point in heat exchangers	ΔT_{pp}	3	K	[10, 12]
HP working fluid	fluid_{hp}	R1233zd(E)	n/a	[10, 12]
Resistive heater thermal efficiency	$\eta^{\text{th}}_{\text{rh}}$	1.0	-	[34]
Hot storage temperature	$T^{\text{max}}_{\text{tes}}$	design var.	°C	n/a
Storage temperature spread	$\Delta T_{\text{tes,sp}}$	design var.	K	n/a
Storage thermal efficiency	$\eta^{\text{th}}_{\text{tes}}$	1.0	-	[19]
Tanks pressure	p_{tes}	7.5	bar	*see Section 2.2.1*
Expander isentropic efficiency	$\eta_{\text{is,exp}}$	0.75	-	[10]
Feed pump isentropic efficiency	$\eta_{\text{is,pmp}}$	0.60	-	[10]
Pressure losses in ORC	Δp_{orc}	0	bar	[12, 13]
Heat sink temperature glide	$\Delta T_{\text{cs,gl}}$	10	K	[22]
ORC vapor superheat	$\Delta T_{\text{orc,sh}}$	max.	K	[35]
ORC liquid subcooling	$\Delta T_{\text{orc,sc}}$	3	K	[13]
ORC working fluid	$\text{fluid}_{\text{orc}}$	R1233zd(E)	n/a	[10, 12]

Table 2: Parameters of the quasi-steady state thermodynamic model used for the Carnot battery. Some parameters are used as design variables and will be further discussed in Section 2.4. The values of $\Delta T_{\text{hp,sc}}$ and $\Delta T_{\text{orc,sh}}$ depend on the boundary conditions but are maximised in any case.

In this model, performance degradation associated with part-load and off-design operations (i.e. variation in pressure losses, efficiency of compression and expansion machines, heat losses, etc.) is not taken into account. Nor are there any constraints on minimum loads. Only maximum loads are restricted by the nominal designs, which result from the optimisation problem presented in Section 2.4. These assumptions are made in order to make the CB sufficiently flexible in the light of the fluctuations in power demand and supply (see Fig. 3) and have also been applied by Tassenoy *et al.* [25]. An analysis of the impact of a constrained minimum power, which is normally encountered in reality, is out of the scope of this study, though it deserves further investigation. In this model, ageing (i.e. performance degradation over the lifetime) is also neglected, assuming a sufficient yearly maintenance (see Section 2.3 for the model of maintenance costs).

The thermal storage is based on pressurized water tanks, with different temperature levels. Water is adopted as storage fluid as it offers a high volumetric thermal capacity at a low cost. The tanks are pressurised to 7.5 bar to allow temperatures up to 150°C. Such high storage temperatures allow larger densities and exergy efficiencies to be reached, as explained in [36]. The 150°C limit is set to ensure lubricant and working fluid stability in the heat pump [12, 13]. Although it is more expensive, the two-tank architecture is preferred to a single tank as it provides a constant thermal profile regardless of the state of charge and storage duration (i.e. no diffusion losses due to a thermocline). Latent heat storage is not considered in this work as it is currently costly and has low power densities [6]. In this model, the storage heat losses are neglected, assuming a sufficient thermal insulation and because the target application is for overnight storage, due to the coupling with PV. This can be justified because less than 0.5% loss per day is usually assumed in very high temperature thermal storage (> 500°C) [27]. This simplification is also introduced to reduce the model complexity and has been used in other studies [19]. Indeed, heat losses in sensible heat storage would imply a decrease in temperature, which would require dynamic considerations in the model and affect the control strategy.

As far as compression and expansion machines are concerned, the considered power range (i.e. ∼100 kW) and the need for flexibility encourages the use of volumetric machines. Specifically, for the ORC, scroll or screw type expanders can be used. The nominal isentropic efficiency of these machines is around 0.75 [10]. For the HP, given the high lifts permitted (i.e. hot storage can reach 150°C while minimum heat source temperature can be -5°C in Louvain-la-Neuve), very high compression ratios may be necessary (e.g. more than 60 with R1233zd(E)). Conservatively, reciprocating compressors that allow such compression ratios seem appropriate, despite their lower efficiency. It should be mentioned again that, in practice, this type of compression would be carried out in several machines, but for a techno-economic study, it can be modelled as a single transformation. Therefore, an isentropic efficiency of 0.65 has been selected to model the compressor [37]. Please note that the sensitivity of the results to this value is tested in the uncertainty analysis (Section 4.2) and indicates that it is not significant in relation to other uncertainties. In more advanced systems, compression could be multi-staged, which would make it possible to reduce the required compression ratios and to use machines with better isentropic efficiencies. Cascaded systems could also be considered.

2.2.2. Photovoltaic array

The PV array is modelled with `PVlib`, an experimentally validated open-source `Python` package [38, 39]. The PV current and voltage are evaluated with the single-diode model,

$$I_{\mathrm{PV}} = I_L - I_0 \exp\left(\frac{U + IR_s}{n_{\mathrm{diode}} N_s U_{\mathrm{th}}} - 1\right) - \frac{U + IR_s}{n_{R_{\mathrm{sh}}}} \quad . \tag{1}$$

The parameters in Eq. 1 are determined with the method developed by De Soto *et al.* [40], based on manufacturer data adopted from a typical monocrystalline silicon PV panel (Sunpower SPR X-19-240-BLK [41]). The efficiency of the DC-AC inverter is assumed to be 1.00. This is a fair assumption considering the efficiencies above 0.95 reported by [42].

2.2.3. Cooling system and auxiliaries

As the consumption data for the air chiller and dry cooler could not be transmitted by the operators of the UCLouvain data centre, a reconstruction technique had to be applied. The curves shown in Fig. 3 have been produced as follows.

For a given cooling demand, the chiller consumption can be assessed by estimating its COP. The latter is obtained based on the boundary temperatures (i.e. hot cooling water and ambient) and using the Carnot efficiency. In this work, the actual chiller is assumed to be

40% Carnot efficient [43]. The dry cooler is a passive component, so its energy consumption for cold production is zero.

Other auxiliaries, like circulating pumps, fans, liquid cooling packages, etc., are not considered in this model. It is assumed that their impact on the techno-economic performance can be neglected at this stage of the investigation of the case study [18, 19].

2.2.4. Key performance indicators

The different performance indicators that are used to analyse the system are assessed on an annual basis. The COP of the HP is defined as

$$\mathrm{COP_{hp}} = \frac{E^{\mathrm{th}}_{\mathrm{hp}}}{E^{\mathrm{el}}_{\mathrm{hp}}} \quad , \tag{2}$$

where $E^{\mathrm{th}}_{\mathrm{hp}}$ is the thermal energy annually produced and $E^{\mathrm{el}}_{\mathrm{hp}}$ the electrical energy annually consumed by the HP. The charging COP of the CB includes the RH, and it is defined as

$$\mathrm{COP_{cb}} = \frac{E^{\mathrm{th}}_{\mathrm{hp}} + E^{\mathrm{th}}_{\mathrm{rh}}}{E^{\mathrm{el}}_{\mathrm{hp}} + E^{\mathrm{el}}_{\mathrm{rh}}} \quad , \tag{3}$$

with $E^{\mathrm{th}}_{\mathrm{rh}}$ and $E^{\mathrm{el}}_{\mathrm{rh}}$ the thermal and electrical energy annually produced and consumed by the RH (in this model, they are equal since $\eta^{\mathrm{th}}_{\mathrm{rh}} = 1$). The ORC efficiency is defined as

$$\eta_{\mathrm{orc}} = \frac{E^{\mathrm{el}}_{\mathrm{orc}}}{E^{\mathrm{th}}_{\mathrm{orc}}} \quad , \tag{4}$$

with $E^{\mathrm{el}}_{\mathrm{orc}}$ and $E^{\mathrm{el}}_{\mathrm{orc}}$ the electrical and thermal energy annually produced and consumed by the ORC. Finally, the electrical efficiency of the CB is defined as

$$\eta_{\mathrm{cb}} = \mathrm{COP_{cb}} \cdot \eta^{\mathrm{th}}_{\mathrm{tes}} \cdot \eta_{\mathrm{orc}} \quad , \tag{5}$$

with $\eta^{\mathrm{th}}_{\mathrm{tes}}$ the efficiency of the TES.

The capacity factors are also useful to quantify the utilisation of the charging and discharging systems. For each technology, these are defined as

$$\mathrm{CF}_i = \frac{E_i}{8760 \cdot P^{\max}_i} \quad , \tag{6}$$

where E_i is the energy annually produced by the technology i and $P_i^{\max}$ its nominal capacity. Last figures are the nominal charge and discharge time of the CB. These are defined as

$$\tau_{\mathrm{ch}} = \frac{E_{\mathrm{tes}}^{\mathrm{th}}}{P_{\mathrm{hp}}^{\mathrm{th,max}} + P_{\mathrm{rh}}^{\mathrm{th,max}}} \quad , \tag{7}$$

$$\tau_{\mathrm{disch}} = \frac{E_{\mathrm{tes}}^{\mathrm{th}} \cdot \eta_{\mathrm{orc}}}{P_{\mathrm{orc}}^{\mathrm{el,max}}} \quad , \tag{8}$$

where $E_{\mathrm{tes}}^{\mathrm{th}}$ is the thermal capacity of the TES.

2.2.5. Power management strategy

To balance the system, a rule-based power management strategy is used at each hour along the year. The latter is depicted in Fig. 4. It should be mentioned that not all the operational details of the system are shown in the diagram (e.g. constraints for maintaining the state of charge ≥ 0 and $\leq 100\%$, ...).

The basic idea behind this strategy is as follows. If the PV overproduces, the CB is charged via the HP. If the HP runs at nominal load, the RH absorbs the remaining power. If any excess power remains, it is sent to the grid. Conversely, when the PV underproduces compared to the power demand, the ORC starts up and attempts to meet the power demand. If it runs at nominal load but does not satisfy the power demand, the remainder is purchased from the grid.

2.3. Economic model

From a technical point of view, the aim of installing a PV + CB system is to minimise the primary energy consumption of the data centre, which is equivalent to maximising its self-sufficiency ratio. However, from an economic perspective, the investment required to deploy such system should be motivated by a financial gain - or at least, no losses.

2.3.1. Net present value and internal rate of return

A common way of comparing the profitability of different investments for a given project is to use the net present value

$$\mathrm{NPV} = -C_0 + \sum_{n=1}^{LT} \frac{B_n - C_n}{(1+r)^n} \quad , \tag{9}$$

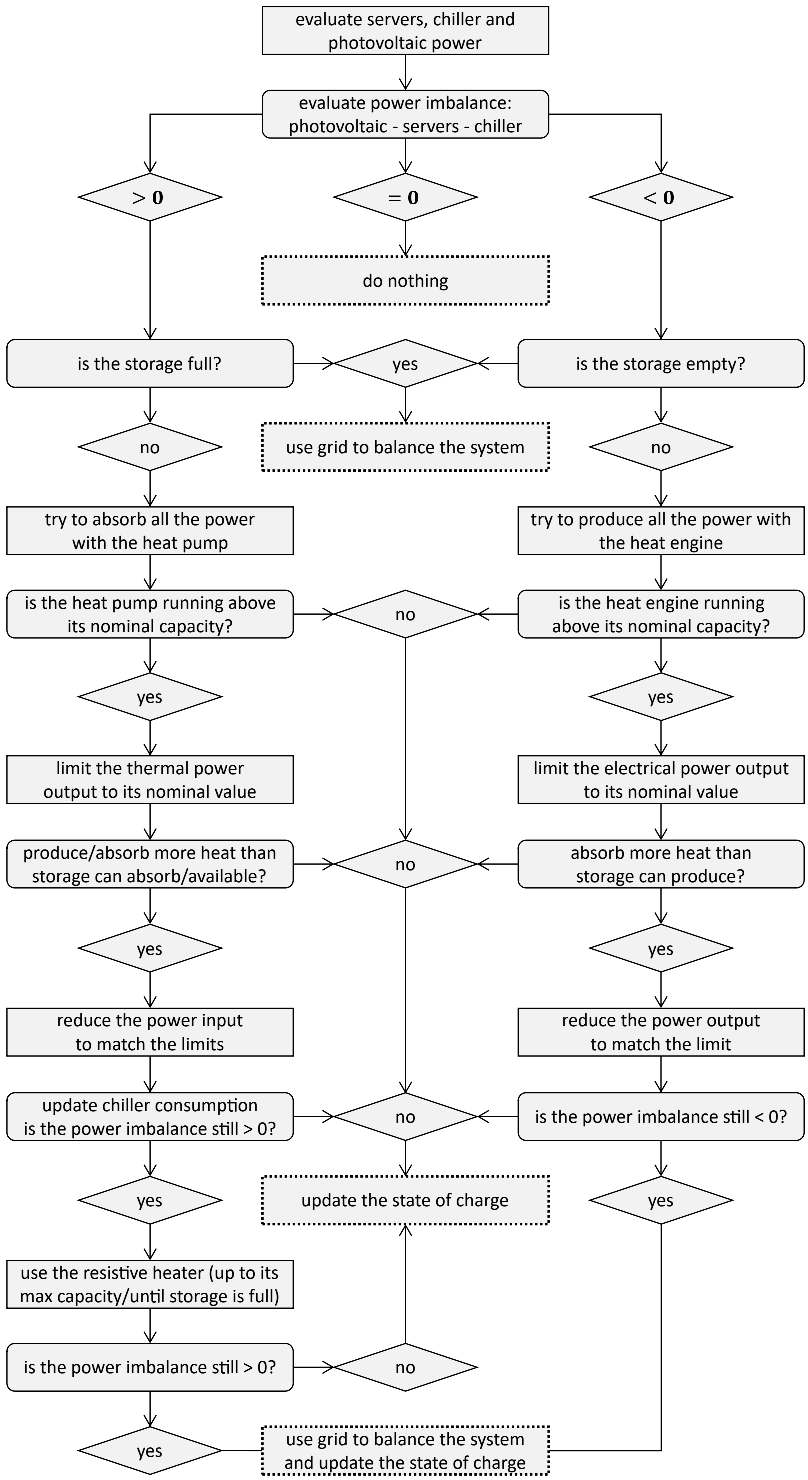

Figure 4: Power management strategy used to balance the power flows in the system at each hour of the year.

where C_0 is the capital cost, B_n and C_n are the annual benefits and costs of the project, and r is the discount rate. It represents the sum of the present values (i.e. difference between incoming and outgoing cashflows) over the lifetime LT of the project. When it is positive (resp. negative), the project yields a higher (resp. lower) rate of return on investment than the prescribed discount rate, so the investment is economically sound (resp. should be avoided).

As the value that the NPV can take on is sometimes difficult to interpret, it can be supplemented by the discounted payback period (DPP). This is defined, for a given discount rate, as the time required to obtain a zero NPV.

The value of the discount rate is typically set to the minimum desired rate of return on investment. In this sense, it must account simultaneously for inflation, for the cost of non-availability of the capital and for the risk of investment [44]. As a result, the value of r is not fixed, but it is specific to each investment strategy.

In order to analyse the economic performance of an investment generically and independently from the possible investment strategies, the internal rate of return (IRR) can also be used. The latter is precisely defined as the discount rate that results in a zero NPV. It quantifies the rate of growth that the project is anticipated to generate [44].

2.3.2. Economic correlations

To assess the NPV and IRR of each design that will be evaluated, the annual costs C_n and benefits B_n, as well as the capital costs C_0, must be defined.

Before going into further detail about the correlations used, it is essential to point out that the values reported in the following are extremely subject to uncertainty. The price of components and energy carriers can vary depending on the manufacturers and the market, especially for a technology that is not yet commercially available. Furthermore, the evolution of these prices over time is also uncertain. As a result, average values are adopted for the economic parameters, so as to reflect the reality of the market objectively and to give a more or less realistic order of magnitude for the financial performance of Carnot batteries. But as these prices are subject to change, a parametric analysis will also be proposed to show the impact of a 50% drop in C_0 ($C_0^{50\%}$) compared to the case with a full C_0 ($C_0^{100\%}$).

In this model, B_n is defined as the difference between the annual cost of electricity when no PV or CB is installed (i.e. the data centre only consumes electricity from the grid) and the annual cost of electricity for the design under test, where some of the electricity is supplied by the PV + CB system (i.e. this cost is lower because less electricity is absorbed from the grid). No subsidies are taken into account. Note that in the present definition of B_n, excess PV generation that is returned to the grid is sold at a zero price. This is a conservative choice, yet it favours the storage of electricity. The average annual electricity prices are modelled considering a linear growth with time as

$$c_{\text{el}}(n) = a_{\text{el}} \cdot n + b_{\text{el}} \quad , \tag{10}$$

where a_{el} is the average annual rate of growth of the electricity price, b_{el} is the average annual electricity price when commissioning the PV + CB system and n an integer representing the year under consideration (see Eq. 9). The coefficients in Eq. 10 are fitted as a linear extrapolation of the Banb IB electricity prices for non-households consumers (i.e. 20 MWh $<$ consumption $<$ 500 MWh) in Belgium and Spain from 2007 to 2021 from the Eurostat database [45]. Their respective values can be found in Table 3. Please note that with this model for c_{el}, an energy arbitrage strategy cannot be implemented.

By fitting the coefficients in Eq. 10 to historical values, the average historical inflation in the price of electricity is extrapolated to the entire lifetime of the system. This model therefore assumes that the price of electricity will continue to rise in the future (without correcting it to express it in € for a particular year) and uses deterministic values to represent it, as the impact of uncertainty on it is outside the scope of this study. Nevertheless, a previous study by the authors has shown that this uncertainty has a non-negligible impact on financial performance of the system [46], and it therefore deserves further investigation using appropriate methods.

In this moel C_n (the OPEX) is represented as a fraction of the total capital costs $\%_{C_0}$ and only accounts for the maintenance (i.e. no reinvestment costs, no taxes). This simplified approach is frequently adopted in the literature as it is difficult to give precise specific maintenance costs for technologies with low readiness levels. In the literature on Carnot batteries, $\%_{C_0}$ ranges from 1.5% [18–20, 25] to 3.0% [17]. In this case, it is set to 2% (see Table 3).

Parameter	Value	Units	Min.	Max.	References
$a_{\text{el,Belgium}}$	2.841	€$_{2021}$/MWh/y	n/a	n/a	[45]
$b_{\text{el,Belgium}}$	195.9	€$_{2021}$/MWh	n/a	n/a	[45]
$a_{\text{el,Spain}}$	2.078	€$_{2021}$/MWh/y	n/a	n/a	[45]
$b_{\text{el,Spain}}$	183.8	€$_{2021}$/MWh	n/a	n/a	[45]
C_n	2.0	$\%_{C_0}$	1.5	3.0	[17–20, 25]
CAPEX_{PV}	870	€$_{2021}$/kWp	400	870	[47, 48]
CAPEX_{HP}	430	€$_{2021}$/kW$_{\text{th}}$	250	720	[17, 49, 50]
CAPEX_{RH}	150	€$_{2021}$/kW$_{\text{th}}$	100	150	[34, 48]
$\text{CAPEX}_{\text{TES}}$	$log(V) - 0.002407V^2$ $+791.4V + 6191$	€$_{2021}$	n/a	n/a	[51]
$\text{CAPEX}_{\text{ORC}}$	2950	€$_{2021}$/kW$_{\text{el}}$	2125	4000	[17, 25, 52]
r	7.0	%	5.0	8.0	[17–20, 25]
LT	20	year	20	25	[17–20, 25]

Table 3: Correlations for the economic model. Note that in this model, the ratio between the HP and RH costs favours the investment in the HP. The dependency variable for the cost of thermal storage is V, the volume of the tanks.

Different approaches exist to evaluate C_0. In some works, the costs of all physical components of the CB (e.g. heat exchangers, compressors, ...) are added together [12, 18–20]. To the best authors' knowledge, with this approach, engineering and assembly costs are hardly considered. Still, one of the advantages of this method is that it enables to assess the impact of each component on the overall cost of the CB, so that detailed cost breakdowns can be evaluated, for example.

A second approach is to only consider the prices of the CB sub-systems (i.e. HP, RH, TES and ORC), and add them together. This method is certainly more conservative because it considers assembly and engineering costs for each sub-system, whereas these could be reduced if the CB was designed as a whole.

It is interesting to note that by using the first or second method, the specific costs of this type of Carnot batteries can vary by more than one order of magnitude, as they range from 500 \$/kW and 250 \$/kWh to 8000 \$/kW and 1000 \$/kWh [1, 16].

Since the second method is more conservative - although probably simplistic - for analysing the integration of CB into existing energy systems, it seems appropriate at this stage of the technology's development, and it is therefore adopted for this work. It was also adopted by Frate *et al.* [17] and Tassenoy *et al.* [25]. The capital cost of the PV + CB system is thus defined as

$$C_0 = \mathrm{CAPEX_{PV}} + \mathrm{CAPEX_{HP}} + \mathrm{CAPEX_{RH}} + \mathrm{CAPEX_{TES}} + \mathrm{CAPEX_{ORC}} \quad . \tag{11}$$

The adopted correlations are given in Table 3, with the associated references.

Note that although these CAPEX are quite uncertain, they must be assigned fixed values in order to carry out the techno-economic analysis. This is not problematic as such, since parametric analyses on these values make it easy to characterise the sensitivity of the economic performance. On the other hand, the uncertainties on the ratios between the different CAPEX (i.e. relative costs between the sub-systems) are more impacting. Indeed, as these cost correlations will be used in an optimisation model, the obtained designs will be biased by these uncertainties. For example, if the RH is relatively too cheap compared with the HP, it could be preferred despite its lower efficiency. To deal with this, methodological innovations based in particular on the principles of robust design optimisation [53] and near optimum analysis are necessary, and will be the subject of future works.

It should be mentioned, however, that this consideration applies with a variable intensity along the Pareto fronts that will result from the compromise between the technical and economic performance. Indeed, for the designs providing the best technical performance (i.e. the data centre energy self-sufficiency), the costs uncertainties no longer have any real impact because those designs will be optimised, above all, to provide the best technical performance, to the detriment of the economic performance.

In Table 3, the cost correlation for HP was obtained by taking the average of the specific prices for commercially available high-temperature heat pumps listed in the IEA Task 58 fact-sheets. The cost correlation for the ORC was obtained by taking the average of the specific costs reported by Lemmens *et al.* [54] for low-power ORC modules. The discount rate is set to 7% so as to conservatively reflect the values recently selected in other techno-economic analyses on CB [17–20, 25].

2.4. Optimisation problem

As mentioned earlier, the goal in this work is to optimise the design of a PV + CB system to maximise the data centre self-sufficiency ratio:

$$\mathrm{SSR} = 1 - \frac{E^{\mathrm{el}}_{\mathrm{grid}}}{E^{\mathrm{el}}_{\mathrm{servers}} + E^{\mathrm{el}}_{\mathrm{chiller}}} \quad , \tag{12}$$

where $E^{\mathrm{el}}_{\mathrm{grid}}$ is the energy annually supplied by the grid and $E^{\mathrm{el}}_{\mathrm{servers}}$ and $E^{\mathrm{el}}_{\mathrm{chiller}}$ are the annual energy consumption of the servers and chiller.

Nevertheless, the investment must remain economically attractive, so it is also necessary to optimise the financial performance of the system. Although the NPV relates the expected gains, it says nothing about the rate of return on investment, whereas this is one of the parameters that investors generally look to first and foremost. Moreover, the NPV requires a discount rate to be set, which is specific to the investment strategy, so it is not possible to characterise the project financial performance independently of it. Consequently, the financial criterion maximised in this work will be the IRR, as it has been introduced in the economic model in Section 2.3.

To maximise the SSR and IRR, the capacity of the PV + CB system can be adjusted. This includes the peak power of the PV system, the nominal power of the HP and RH, the volume of the tanks for thermal storage and the rated power of the ORC. The thermodynamic cycle of the CB can also be adjusted to maximise the SSR or the IRR. Indeed, the "Carnot battery trilemma" [13] indicates that it is not possible to design a CB that maximises both the storage efficiency (the SSR for a given PV capacity) and the energy density (the storage volume), which affects the CAPEX and thus the IRR [13, 36]. Therefore, in this model, it is also possible to optimise the hot temperature of the thermal storage as well as its spread (i.e. the temperature difference between the two tanks). The optimisation variables and corresponding bounds are shown in Table 4.

Optimisation variable	**Symbol**	**Min**	**Max**	**Units**
PV system peak capacity	$P_{pv}^{el,max}$	0	1000	kW_p
HP nominal capacity	$P_{hp}^{th,max}$	0	n/a	kW_{th}
RH nominal capacity	$P_{rh}^{th,max}$	0	n/a	kW_{th}
ORC nominal capacity	$P_{orc}^{el,max}$	0	n/a	kW_{el}
Pressurized tanks volume	V_{tes}	0	n/a	m^3
Hot storage temperature	T_{tes}^{max}	75	150	°C
Storage temperature spread	$\Delta T_{tes,sp}$	10	100	K

Table 4: Optimisation variables and associated design space. If the optimiser tests a physically inconsistent set of TES temperatures, the design is rejected.

In Table 4, the maximum bound on $P_{pv}^{el,max}$ makes it possible to show the interesting case where, when all the PV capacity is installed, the only option for increasing the SSR is to increase the storage capacity, as will be illustrated below.

A novelty of this model compared with other techno-economic studies on CB, is that it simultaneously optimises the cycle and the capacity of the CB in order to maximise its performance. This makes the problem highly non-linear and complex, since some variables have much less impact than others on SSR and IRR. For example, $\Delta T_{tes,sp}$, which influences the storage efficiency and density, will have to interact with V_{tes}, but it will have an indirect impact on SSR and IRR. On the other hand, $P_{orc}^{el,max}$ will have a much more direct impact on these two criteria. Another example of complementary variables is $P_{hp}^{th,max}$ and $P_{rh}^{th,max}$: the algorithm will have to optimise these simultaneously.

In this work, the non-dominated sorting genetic algorithm NSGA-II [55] has been used to handle the multi-criteria optimisation problem. This meta-heuristic algorithm was selected because it performs well in optimising energy systems [39, 56, 57], and because it comes with the `RHEIA` framework [53], which is used for the uncertainty analysis (see Section 2.5). It should be noted that multi-objective particle swarm optimisation (MOPSO) could also have been used, as its performance is similar to that of NSGA-II in this type of problem [57]. Although the improved strength Pareto evolutionary algorithm (SPEA-2) could also represent an interesting alternative, it was unfortunately not tested here.

For each case study, the population size is set to 60. The crossover probability is 0.9, the mutation probability is 0.1 and the crowding degree is 0.2. There is no limit on the number of generation: the optimisation process is stopped when satisfactory results are obtained.

2.5. Uncertainty quantification

The integration scenarios tested in this work face techno-economic uncertainties. The economic uncertainties affect the IRR and some of them will be addressed thanks to the parametric study on C_0. To validate that technical and operational uncertainties do not affect the conclusions drawn about the designs maximising the SSR, they will also be taken into account. These relate to machine efficiencies, heat exchanger pinch-points and time series. The list of uncertainties considered in this model is shown in Table 5, together with their associated values.

To assess the impact of these uncertainties on the SSR, they are propagated in the model using non-intrusive Polynomial Chaos Expansion through the `RHEIA` framework [53]. Compared with conventional Monte Carlo simulations, Polynomial Chaos Expansion achieves accurate statistics in less computational time. It also allows to directly deduce various statistical moments, such as the mean and standard deviation, or the Sobol' indices, which represent the contribution of each parameter to the overall uncertainty.

Parameter	Symbol	Deviation	Units	Distribution
Compressor isentropic efficiency	$\eta_{\mathrm{is,comp}}$	0.05	-	Uniform
Expander isentropic efficiency	$\eta_{\mathrm{is,exp}}$	0.05	-	Uniform
Feed pump isentropic efficiency	$\eta_{\mathrm{is,pmp}}$	0.05	-	Uniform
Pinch point in heat exchangers	ΔT_{pp}	1.5	K	Uniform
Carnot efficiency of chiller	$\eta_{\mathrm{Carnot}}^{\mathrm{chiller}}$	0.05	-	Uniform
Servers power	$P_{\mathrm{servers}}^{\mathrm{el}}$	5.0	%	Gaussian
Cooling water temperature	T_{coolant}	0.2	°C	Gaussian
Solar irradiance	G	7.0	%	Gaussian
Ambient temperature	T_{ambient}	1.0	°C	Gaussian

Table 5: List of uncertainties affecting the SSR. Note that the uncertainty on the servers power affects the cooling system accordingly. The ranges for $\eta_{\mathrm{is,comp}}$, $\eta_{\mathrm{is,exp}}$, $\eta_{\mathrm{is,pmp}}$ and ΔT_{pp} cover values that can be encountered in real machines and are used to assess the sensitivity of the SSR to them. The value of $\eta_{\mathrm{Carnot}}^{\mathrm{chiller}}$ is from [49]. Values for $P_{\mathrm{servers}}^{\mathrm{el}}$ and T_{coolant} are from the historical data of the data centre. Values for G and T_{ambient} are from [39].

3. Results of multi-criteria optimisation

3.1. Pareto fronts

The Pareto fronts resulting from the multi-criteria optimisation between the IRR and the SSR are depicted in Fig. 5. For each of the three scenarios in Louvain-la-Neuve and Seville, two lines are plotted: the solid lines represent the case $C_0^{100\%}$, and the dashed lines represent the case $C_0^{50\%}$ ($\mathrm{CAPEX_{PV}}$ is unchanged). This parametric analysis illustrates the potential financial gains if the investment costs in the Carnot battery were to fall. It will be further explored in Section 3.6.

Regarding the minimum IRR values, when these are negative, it means that it is not possible to find a discount rate giving a zero NPV for the allotted lifetime. The discount rate must therefore become negative to obtain a zero NPV. It is worth mentioning here that a ”capacity remuneration mechanism” should be provided, as we are seeking to achieve higher SSR in order to limit the impact on the grid.

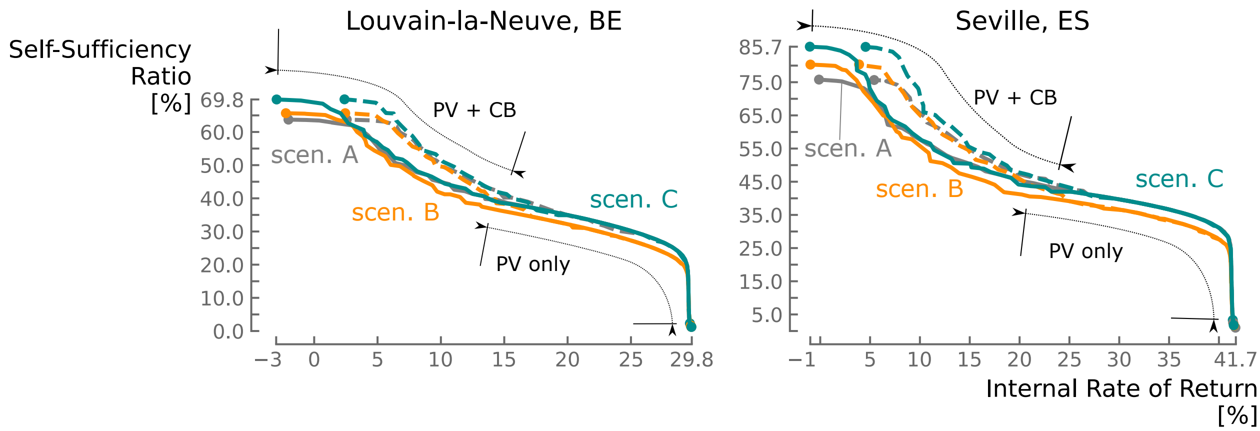

Figure 5: Pareto fronts resulting from the optimisation between the Internal Rate of Return and the Self-Sufficiency Ratio. In each scenario, the solid curves result from the case $C_0^{100\%}$. The dashed curves correspond to the case $C_0^{50\%}$.

Another observation is that, for the designs achieving higher IRR, the cases $C_0^{50\%}$ and $C_0^{100\%}$ offer the same SSR in scenarios A and C (i.e. the curves overlap). It is slightly lower in scenario B, only because the zero consumption of the chiller affects the ratio defined in Eq. 12. In fact, as this will be illustrated in Section 3.2, these designs do contain only PV, which has the same CAPEX in both cases. Then, as the SSR increases, storage gets deployed for the case $C_0^{50\%}$ when the solid and dashed lines separate, since the same investment costs as in case $C_0^{100\%}$ lead to designs providing higher SSR (i.e. they include storage).

It must also be noted that Seville offers larger IRR and SSR than Louvain-la-Neuve. This is mostly due to the difference in PV capacity factor, which is almost 50% higher in Seville than in Louvain-la-Neuve (i.e. 22.9% against 15.4%), thanks to the higher solar irradiance.

To better discriminate the performance of the different scenarios and to ease their analysis, Fig. 6 shows a zoom on the designs that include storage. These enlarged fronts show that the SSR has an asymptotic relation with the IRR, and that scenario C always performs better than B and A, despite it has no thermal integration. They also show that, for a given SSR, $C_0^{50\%}$ provide greater IRR than $C_0^{100\%}$, as expected. These findings are discussed in the following.

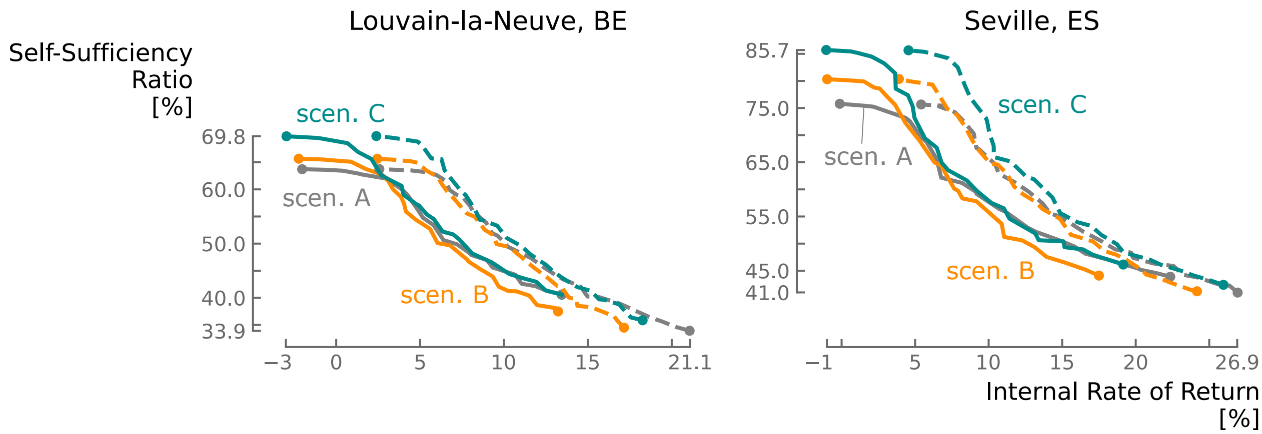

Figure 6: Zoom on Pareto fronts where the designs include storage. It can be seen that the higher the SSR, the more the reduction in the Carnot battery CAPEX enables the IRR to be increased (i.e. the horizontal distance between the solid and dashed curves increases with the SSR).

3.2. Asymptotic fronts: a matter of installed capacity

It can be observed in Fig. 6 that, when reaching high SSR, the fronts take an asymptotic profile with the IRR. As illustrated in Fig. 7, this is because once the maximum PV capacity is installed with the associated optimum storage capacity (i.e. 1000 kWh in Louvain-la-Neuve and 1500 kWh in Seville), the last percentages in SSR are gained at the cost of an oversized storage capacity (in terms of financial gains), which ultimately leads to exponentially increasing costs. This exponential growth in storage capacity also indicates that the system shifts from overnight storage to longer-term storage. It is interesting to note that, as with the PV capacity factor, the optimum storage capacity is 50% higher in Seville than in Louvain-la-Neuve. This perfectly illustrates the direct relationship between these two design variables.

As mentioned earlier, the designs leading to highest IRR do not include storage but only PV. However, it is worth noting that, both in Louvain-la-Neuve and Seville, once the optimum standalone PV capacity is installed (i.e. about 500 kW in Louvain-la-Neuve and 400 kW in Seville), the increase in SSR goes along with a simultaneous increase in CB and PV capacities. This means that, for the considered CB and PV capital costs, the most cost effective solution to increase the SSR is to include storage. Of course, these results are

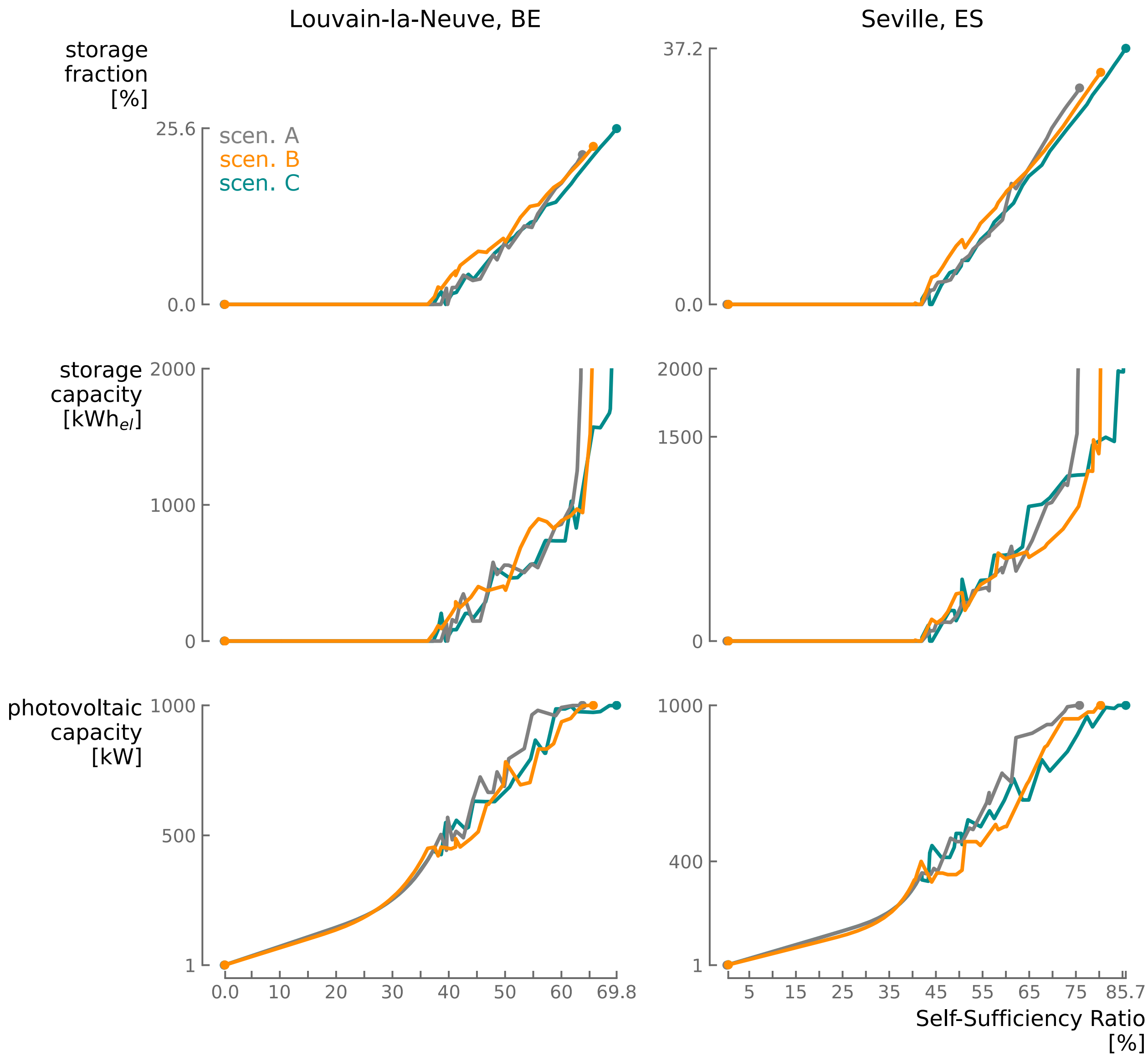

Figure 7: Relationship between the PV and storage capacities with the SSR. The storage fraction shows the share of electricity that was annually supplied to the data centre directly from the CB. Please note that the storage capacity is truncated at 2000 kWh$_{el}$ for the sake of clarity, but may be higher locally. The trends of the results obtained for the case $C_0^{50\%}$ are not represented for the sake of clarity, but they are very similar since only the technical aspects influence the SSR. The only difference is that storage gets deployed starting from lower SSR since the costs are lower.

specific to the economic model utilised here: if PV was to be cheaper, the most economically profitable solution would include less storage to increase the SSR (up to the maximum PV capacity). Conversely, in the case $C_0^{50\%}$, storage is installed starting from lower SSR (not represented in Fig. 7 for the sake of clarity, but well visible in Fig. 6).

Fig. 7 also depicts the "storage fraction", the fraction of energy annually supplied to the data center that was actually released by the Carnot battery. Its maximum value is 25.6% in Louvain-la-Neuve and 37.2% in Seville (which is also 50% higher). As the PV capacity increases, the storage fraction always has a linear relationship with the SSR, and also with the storage capacity. When the maximum PV capacity is installed, the storage capacity has an exponential relationship with the storage fraction.

It should finally be observed that the curves are much smoother when only PV is installed, but they get noisier as storage is deployed. This illustrates well the complexity of this optimisation problem: different designs can lead to very similar performance in terms of IRR and SSR, and convergence is therefore difficult, as explained in the optimisation problem (see Section 2.4).

3.3. Maximum SSR in the different scenarios: a matter of thermal booster

As seen in Fig. 6, when the SSR is maximised, scenario C provides the best performance, ahead of scenario B which itself dominates scenario A. The difference in maximum SSR between scenarios C and A is 6.1% in Louvain-la-Neuve and 9.9% in Seville. This result, which may seem counter-intuitive since scenario B theoretically achieves the best storage efficiency (i.e. the average heat source temperature is the highest in scenario B, and lowest in C), can be explained by analysing the design of the charging and discharging systems.

One way of maximising the SSR for a given PV capacity is to increase the storage efficiency and the nominal power of the charging system, as illustrated in Fig. 8. In this context, using an HP gives a higher charging COP than using a RH. However, in scenarios A and B, the amount of thermal power available at the source is limited by the operations of the servers. Since the thermal output is the sum of the power from the heat source and the electricity driving the HP, when the COP increases while keeping a constant thermal power from the source, the thermal output decreases. Consequently, the amount of thermal power that can be produced by the HP is also constrained, and this is all the more true when the COP is high (i.e. scenario B is even more constrained than scenario A).

Therefore, to charge more energy into the storage, a "booster", which is not constrained by the waste heat availability, must be added. In this case, the RH can be used at the cost of a reduced charging COP. It is clear that there is a trade-off to be found between the charging capacity and the COP of the charging system.

Scenario C, however, does not fall into this dilemma. As its heat source is ambient air, it is not constrained and can afford to use only an HP as charging system. Consequently, the best charging COP is obtained in scenario C. Next comes scenario B, which benefits from a source at 60°C, and finally scenario A, whose source is at 24°C.

This reasoning is illustrated in Fig. 8, which shows the thermal capacity of the charging system, the ratio between the thermal capacities of the HP and the RH, and the COP of the charging system.

Note that both in Seville and Louvain-la-Neuve, when the SSR is high, the charging COP for scenarios A and B are very close to each other. The reason why $\mathrm{SSR}_{\mathrm{B}}^{\mathrm{max}} > \mathrm{SSR}_{\mathrm{A}}^{\mathrm{max}}$ is actually that the amount of available photovoltaic electricity is higher in case B than A, because in scenario B the chiller consumption is always zero, leaving more energy for storage and therefore increasing the SSR.

It is also interesting to note that scenario B, which initially benefits from a large COP, is the only one that is constrained to reduce it in order to increase the thermal power of the charging system. It should be noted, however, that this result must only be analysed qualitatively, as it is specific to the cost correlations used in this model, which are in favour of the HP (i.e. $\mathrm{CAPEX}_{\mathrm{RH}}$ is relatively high compared to $\mathrm{CAPEX}_{\mathrm{HP}}$ that is rather low).

This analysis of the charging system of the thermally integrated Carnot battery shows that its capacity needs to be increased to store more energy and make the system more relevant (i.e. a sufficient fraction of the energy consumed should come from storage to justify

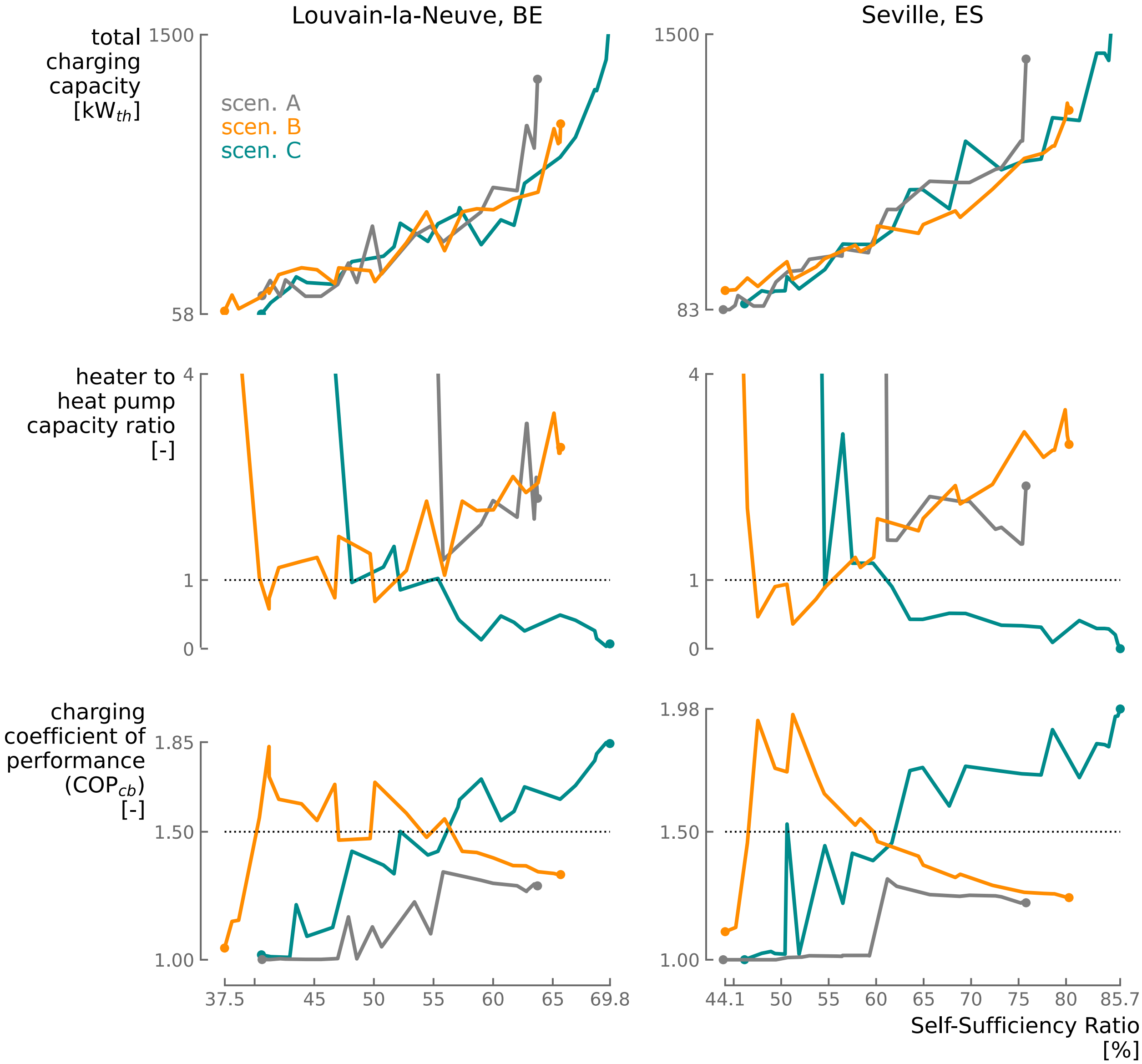

Figure 8: Performance of the charging system in the different scenarios. Please note that the heater to heat pump capacity ratio is only shown up to 4 for the sake of clarity, but locally reaches higher values. In scenario C, the charging COP is higher in Seville than Louvain-la-Neuve thanks to the higher ambient temperature. It can also be seen that for low SSR, the heater is still used in scenarios A and C, and is therefore the best techno-economic compromise. Scenario B needs to decrease its charging COP to increase the charging capacity.

the investment). To illustrate that, this textbook case uses an electric booster, which greatly affects the COP. Therefore, new hybrid charging systems, such as dual heat source HP, should be investigated for Carnot batteries. This will be the subject of future work.

3.4. Synergies between booster, storage efficiency and storage density

As mentioned above, to increase the SSR when the maximum PV capacity is installed, the storage efficiency and the amount of energy stored must be increased. However, as it has just been illustrated, when increasing the amount of energy stored (i.e. the charging capacity), the use of a booster causes the charging COP to fall in scenario B, and prevents it from sufficiently rising in scenario A. Therefore, to avoid a drop in the CB efficiency, which would prevent the SSR from increasing, the efficiency of the discharge cycle must increase.

Since the storage temperature is always maximised in all scenarios to maximise the CB efficiency [36], the last lever to increase the efficiency of the ORC is to reduce the temperature spread of the thermal storage (the evaporation temperature being higher). The consequence of this is to reduce the storage density. However, as explained earlier, to increase the SSR, larger storage capacities are needed. This consideration leads inexorably to an exponential growth in the necessary storage volume, which greatly affects the system cost. This analysis is illustrated in Fig. 9.

Once again, it is interesting to note that scenario C is not subject to this trend: as its COP only increases with rising SSR, it is not forced to simultaneously improve the efficiency of the discharge cycle, which means that the storage density and the ORC efficiency can remain constant. It should also be pointed out that the ORC efficiency of is slightly lower in Seville because the ambient temperature is higher there.

3.5. Waste heat recovery and reduction of chiller consumption

When integrating CB in data centres, the aim is to simultaneously recover the waste heat and to reduce the electricity consumption linked to the cold production, necessary to evacuate it. Fig. 10 illustrates the CB performance with regard to these issues.

It is interesting to note that the chiller consumption can be reduced by more than 50% in scenario A in Louvain-la-Neuve and Seville, what is equivalent to reductions of -3.9% and -7.4% respectively in the total energy consumption of the data centre.

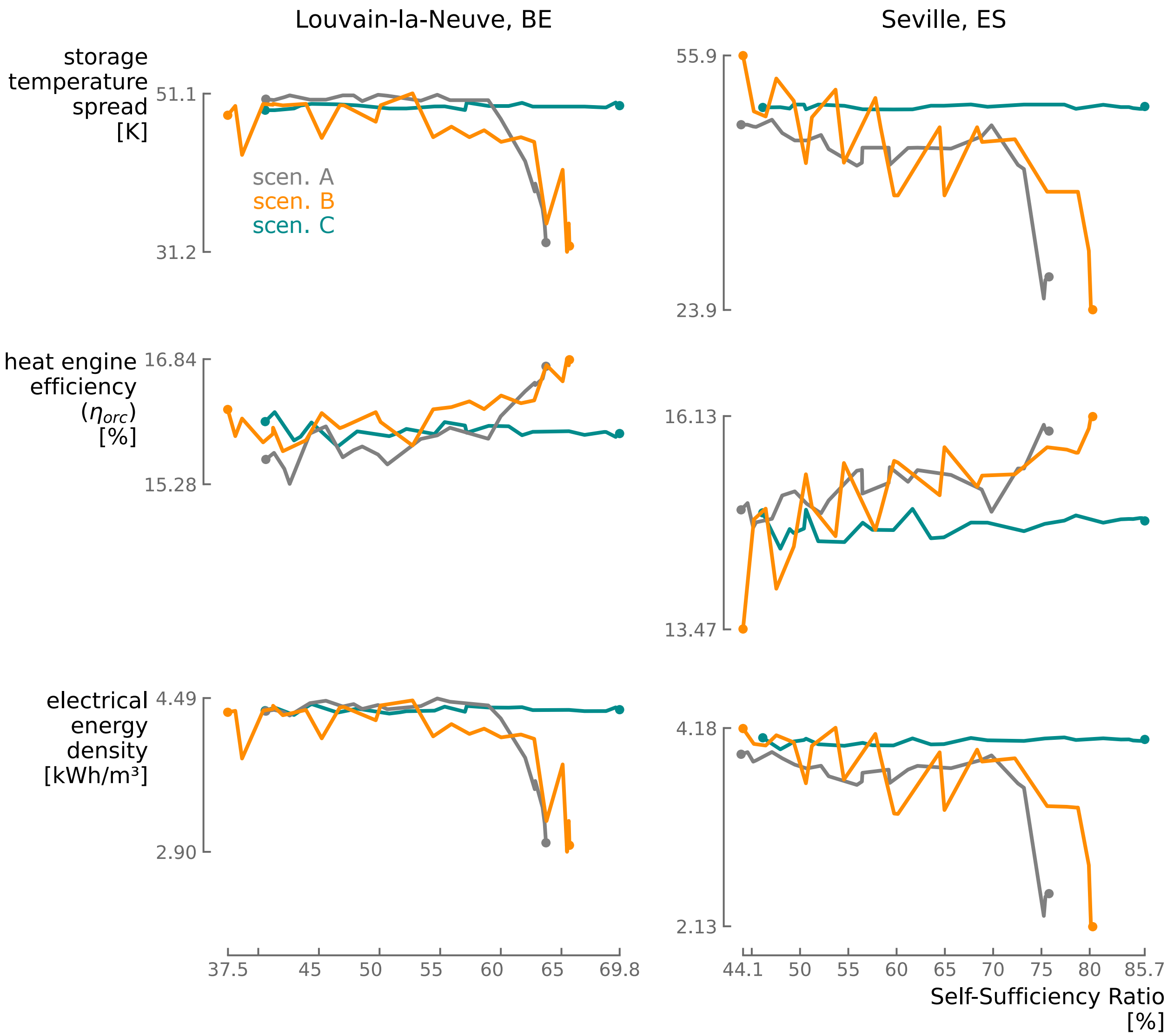

Figure 9: Performance of the storage and discharging systems in the different scenarios. In scenarios B and C, the impact of varying storage temperature spreads is readily apparent in both the efficiency of the ORC and the electrical energy density of the storage. The stronger fluctuations for scenario B in Seville are attributed to a lower level of convergence.

Also, the fraction of waste heat recovered does not exceed 40% in the best case. This is obviously constrained by the availability of PV power, which is already relatively abundant compared with the consumption of the data centre (i.e. there is a ratio of about 2.2 between the PV energy annually produced and that consumed by the servers in Seville) but seems to be an upper limit to bear in mind for this case study. To improve this recovery fraction,

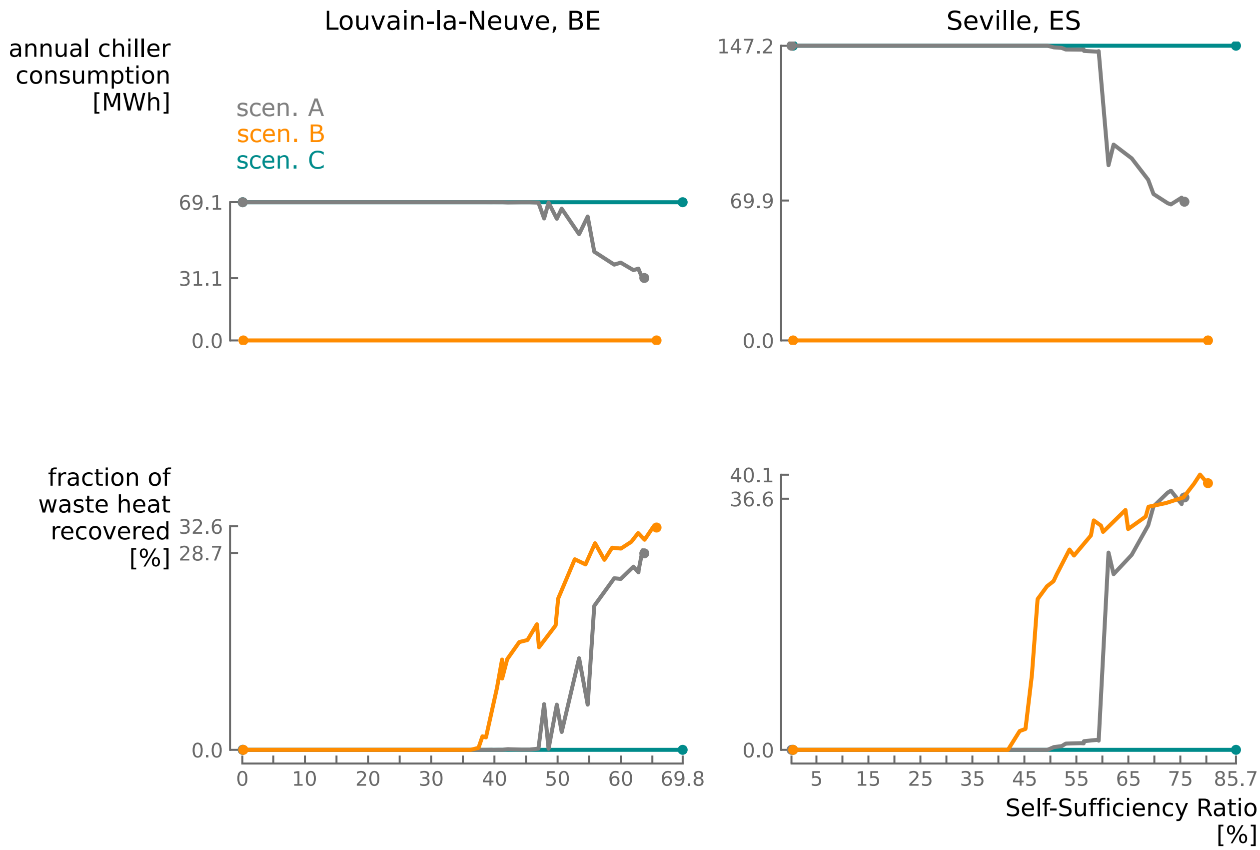

Figure 10: Chiller consumption and waste heat recovery in the different scenarios. In the best cases, reducing the chiller consumption thanks to CB can reduce the data centre energy consumption by 3.9% in Louvain-la-Neuve and 7.4% in Seville.

the charging period would need to be extended. This could be done by positioning the PV panels in different orientations in order to spread out peak production. However, a fraction of 100% is not conceivable, as it would mean that the CB is constantly charging. If charging and discharging times of 12 hours were considered, a maximum waste heat recovery fraction of 50% could be expected.

3.6. Discounted payback period and net present value

The NPV and DPP are depicted for $C_0^{100\%}$ and $C_0^{50\%}$ in Fig. 11.

The first observation is that, for designs including only PV, the DPP remains almost constant as the SSR increases. This trend corresponds to the vertical part of the front in Fig. 5. At the same time, the NPV increases. Then, while storage gets deployed and as the

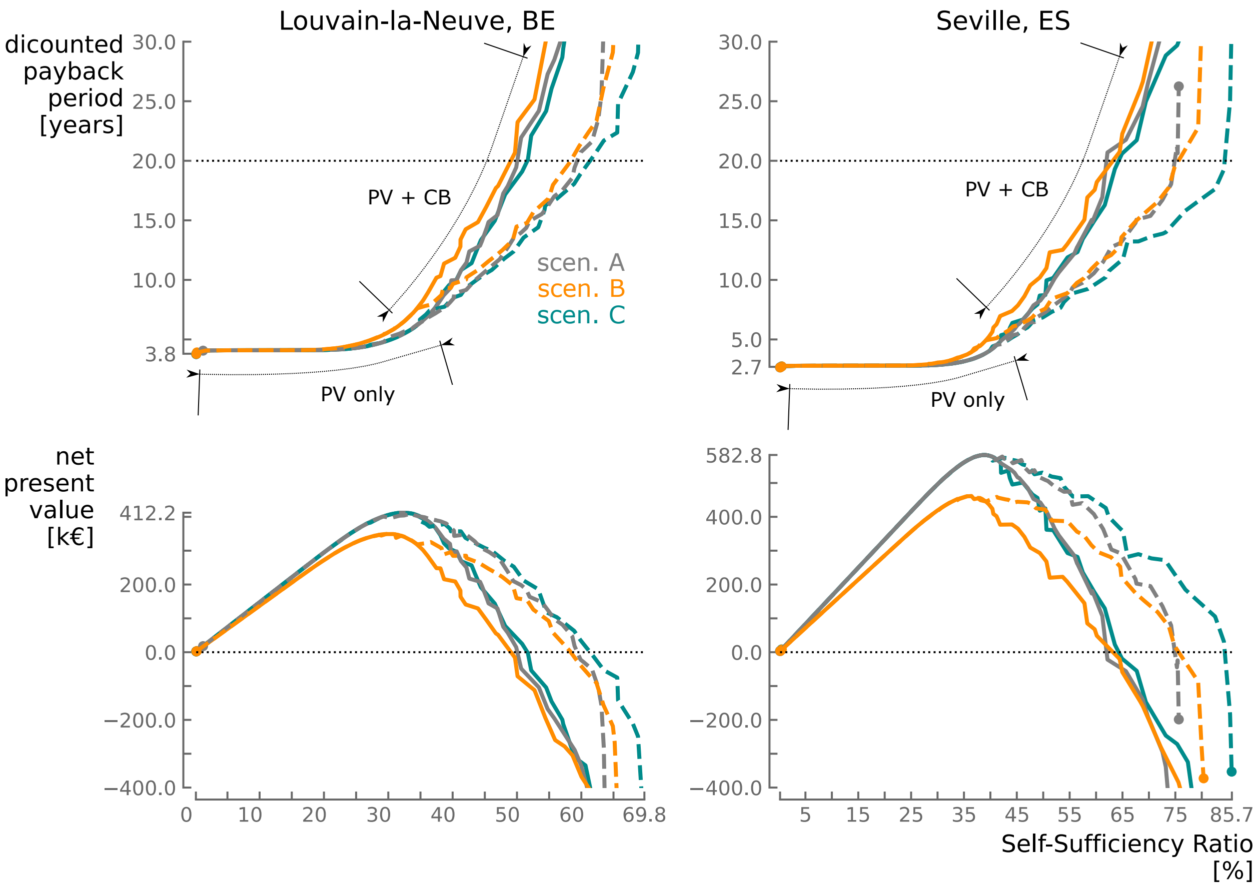

Figure 11: Net present value and discounted payback period of the different designs for $C_0^{100\%}$ and $C_0^{50\%}$.

SSR increases, the DPP starts to increase exponentially. For the last percentages of SSR, it even goes beyond the lifetime of the project. In other words, it is once again shown that when all the PV capacity is installed, the gain in the last few percent in SSR leads to an exponential fall in NPV.

Secondly, the NPV has a bell shape with the SSR. This illustrates that designs with and without storage can give rise to the same financial gains, while those with storage achieve much higher SSR. The downside is that designs that include storage require longer payback periods.

Assuming that grid energy has a non-zero carbon-intensity, a parallel can be drawn between self-sufficiency ratio and decarbonisation. The message that then emerges from Fig. 11 is that an investment strategy aimed at maximising the rate of return on investment does not achieve effective decarbonisation, whereas a strategy that tolerates a lower rate of return offers greater decarbonisation while offering the exact same financial gains.

A final observation shows that, for an equivalent SSR, case $C_0^{50\%}$ gives rise to DPP up to twice as short as case $C_0^{100\%}$, and that this difference increases as the SSR increases. This is perfectly logical since, as illustrated in Fig. 7, the fraction of the energy supplied by the storage to the data center gets higher as the SSR increases, so the effect of a cost reduction is higher.

4. Detailed designs and sensitivity analyses

4.1. Key performance indicators

For each scenario of case $C_0^{100\%}$, one design from the Pareto front is analysed in greater depth to characterise its key performance indicators (KPI) and clarify its role in the energy system. The six designs selected are those for which the maximum PV capacity is installed with the associated financially optimal CB capacity (see Section 3.2 for more details). Technical performance is shown in Table 6 and economic performance is shown in Table 7.

From the results given in Table 6, the first observation is that, although COP_{hp} is maximum in scenario B, COP_{cb} is maximum in scenario C. Consequently, η_{cb} is always better in scenario C, even though η_{orc} is worse because of the higher storage temperature spread. This explains why scenario C has the best SSR for the same PV capacity. It should also be noted that η_{cb} is generally very similar in scenarios A and B. The reason why scenario B has a better SSR is actually due to the fact that the energy consumption of the data centre is lower as the chiller is not used. Finally, we can see that η_{orc}, and consequently η_{cb}, are higher in Louvain-la-Neuve than in Seville because the ambient temperature is lower there.

The second observation is that the nominal charge time is always shorter than the discharge time. Moreover, this charging time is longer in Seville than in Louvain-la-Neuve. This is essentially due to the sunshine duration, which is longer in the south. As far as discharge time is concerned, the main reason why it is usually higher than ten hours is due to a quest

Location	**Louvain-la-Neuve**			**Seville**		
Scenario	**A**	**B**	**C**	**A**	**B**	**C**
SSR	62.0%	65.1%	68.5%	73.2%	78.8%	84.1%
COP_{hp}	1.76	2.55	1.84	1.75	2.49	1.97
COP_{cb}	1.29	1.34	1.78	1.25	1.26	1.84
η_{orc}	16.4%	16.6%	15.9%	15.5%	15.7%	14.8%
η_{cb}	21.2%	22.1%	28.3%	19.3%	19.7%	27.3%
τ_{ch}	8.9h	9.0h	8.6h	9.1h	10.2h	9.5h
τ_{disch}	9.7h	13.2h	12.9h	10.4h	13.0h	15.8h
CF_{hp}	27.8%	25.0%	16.7%	32.3%	30.0%	24.4%
CF_{rh}	13.5%	10.3%	2.6%	21.4%	20.2%	6.4%
CF_{orc}	20.1%	19.9%	20.6%	29.1%	29.0%	33.8%
$frac_{hp}$	51.8%	41.4%	96.0%	46.0%	34.3%	92.8%
$frac_{cb}$	19.8%	22.4%	24.3%	29.0%	32.3%	35.6%
$frac_{whr}$	26.7%	32.4%	0.0%	37.8%	40.1%	0.0%

Table 6: Technical KPI for the designs with maximum PV capacity and financially optimum CB capacity. $frac_{hp}$, $frac_{cb}$ and $frac_{whr}$ are respectively the fractions of thermal energy charged by the HP into the TES (i.e. $1 - frac_{hp} = frac_{rh}$), of electrical energy supplied to the data centre by the CB and of waste heat that is recovered.

to maximise the ORC capacity factor, as this component has a high specific cost. This is in agreement with the results of [25]. Finally, capacity factors are higher in Seville than in Louvain-la-Neuve, thanks to the greater availability of photovoltaic energy.

A final analysis shows that $frac_{hp}$, the fraction of stored heat coming from the HP, is slightly higher in Louvain-la-Neuve than in Seville. This is again explained by the availability of photovoltaic energy: the electric booster is less used in Louvain-la-Neuve because less electricity is available. The proof is that CF_{rh} is always lower in Louvain-la-Neuve than in Seville. Also, $frac_{hp}$ is lower in scenario B than in scenario A. This is due to the fact that COP_{hp} is better in B than in A, and that, consequently, for the same quantity of electricity, less heat can be produced by the HP in scenario B.

Location	Louvain-la-Neuve			Seville		
Scenario	A	B	C	A	B	C
$C_0^{\mathrm{PV+CB}}$ [M€$_{2021}$]	1.568	1.755	2.022	1.659	1.748	2.152
$\mathrm{frac}_{\mathrm{pv}}$	55.4%	49.6%	43.0%	52.2%	48.5%	40.4%
$\mathrm{frac}_{\mathrm{hp}}$	6.5%	5.6%	20.5%	7.6%	5.8%	21.7%
$\mathrm{frac}_{\mathrm{rh}}$	4.4%	6.7%	1.9%	4.7%	5.9%	2.2%
$\mathrm{frac}_{\mathrm{tes}}$	14.0%	18.7%	15.7%	16.0%	20.6%	18.5%
$\mathrm{frac}_{\mathrm{orc}}$	19.7%	19.4%	19.0%	19.5%	19.2%	17.2%
$C_{\mathrm{power}}^{\mathrm{CB}}$ [€$_{2021}$/kW]	6675	7679	8863	7243	7925	10235
$C_{\mathrm{energy}}^{\mathrm{CB}}$ [€$_{2021}$/kWh]	690	582	688	694	610	646

Table 7: Economic KPI for the designs with maximum PV capacity and financially optimum CB capacity. $\mathrm{C}_{\mathrm{power}}^{\mathrm{CB}}$ and $\mathrm{C}_{\mathrm{energy}}^{\mathrm{CB}}$ are the power and energy specific costs of the Carnot battery. The different frac represent the cost breakdown of the total investment cost $C_0^{\mathrm{PV+CB}}$ between the different sub-systems.

The economic analysis shows that, for the same scenario, the distribution of costs between the different sub-systems is very similar in Louvain-la-Neuve and Seville. This tends to show that, when the aim is to maximise the SSR and the IRR, the optimal distribution of investment costs in the PV + CB system is a priori independent from the climatic conditions.

As for the resulting power and energy specific costs, these seem close to the upper bounds anticipated in the literature. As a reminder, these range from 500 to 8000 \$/kW and from 250 to 1000 \$/kWh [1, 16]. Consequently, the economic model used here makes it possible to give sufficiently conservative values. These specific costs are relatively high compared to other storage technologies (e.g. Li-ion is currently $<$ 150 €$_{2021}$/kWh [58]). However, it is difficult to attribute the cause to a single component of CB. Indeed, when the designs include a large HP (i.e. scenario C), the costs seem to be distributed more or less equally between the HP, the TES and the ORC. Note, however, that the contribution of the TES seems to be slightly lower. Therefore, considering these specific costs and those of the literature, the case $C_0^{50\%}$ seems quite reasonable.

Finally, due to its greater use of HP instead of RH, scenario C always gives rise to higher power specific costs and higher investment costs.

4.2. Uncertainty analysis

An uncertainty analysis is also conducted on the SSR. The idea is to verify that the technical and operational uncertainties do not affect the conclusions drawn above.

The uncertainties reported in Table 5 have been propagated in the designs discussed in Section 4.1. Their impact on the SSR is illustrated in Fig. 12 as a 95% confidence interval. It is observed that, although the standard deviations have slightly different amplitudes, these uncertainties affect the SSR in a similar way. Scenario C continues to perform better than B, and the latter better than A.

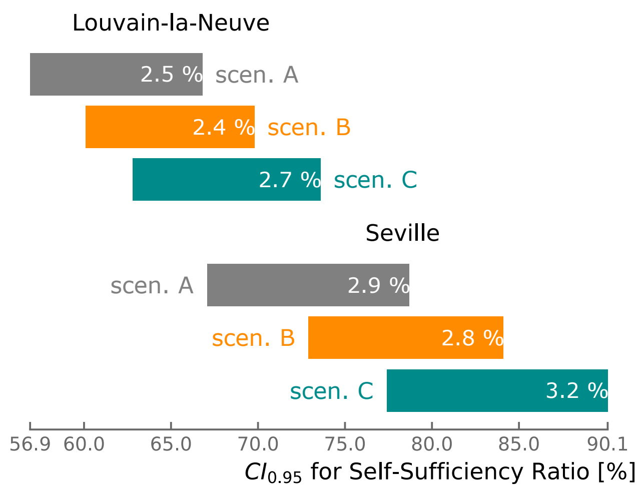

Figure 12: 95% confidence interval for the SSR when propagating the uncertainties reported in Table 5. The values within the bars correspond to the standard deviations.

The observation that emerges from Fig. 12 is that, on average, the higher the SSR, the greater the uncertainty about it, because the higher the SSR, the more the energy system is sensitive to externalities (e.g. photovoltaic production). To verify this and understand precisely what parameters affect the SSR, the most important Sobol indices are reported in

Table 8. These represent the contribution of the considered parameter to the variance of the SSR.

Location	**Louvain-la-Neuve**			**Seville**		
Scenario	**A**	**B**	**C**	**A**	**B**	**C**
1st parameter	G	G	G	G	G	G
Sobol index	46.7%	58.5%	54.3%	40.7%	52.9%	42.6%
2nd parameter	$P^{\text{el}}_{\text{servers}}$	$P^{\text{el}}_{\text{servers}}$	$P^{\text{el}}_{\text{servers}}$	$P^{\text{el}}_{\text{servers}}$	$P^{\text{el}}_{\text{servers}}$	$P^{\text{el}}_{\text{servers}}$
Sobol index	39.0%	31.7%	35.2%	34.1%	32.9%	40.6%
3rd parameter	$\eta_{\text{is,exp}}$	$\eta_{\text{is,exp}}$	$\eta_{\text{is,exp}}$	$\eta_{\text{is,exp}}$	ΔT_{pp}	ΔT_{pp}
Sobol index	6.0%	6.1%	4.5%	10.5%	8.8%	6.2%

Table 8: Sobol indices of the uncertain parameters having the most significant influence on the variance of SSR. The uncertainty over SSR is clearly due first to the uncertainty over photovoltaic production and second to the servers consumption.

In Table 8, it can first be noted that the solar irradiance is the parameter to which the SSR is most sensitive, closely followed by the power of the servers. The technical parameters of the Carnot battery only come in third place and have much lower magnitudes. This illustrates that the precision of the thermodynamic model used here is probably sufficient with regard to the objectives of the techno-economic study.

Another observation is that Louvain-la-Neuve tends to be more sensitive to the uncertainty on the solar irradiance than Seville. This is most likely due to its lower abundance there.

5. Conclusions

This work looked at the techno-economic potential of Carnot batteries coupled to photovoltaic systems and integrated into data centres. The aim is to recover the waste heat they generate and to reduce their cooling consumption. For three different types of thermal integration and two sets of climatic conditions, multi-criteria optimisation was carried out in order to maximise the energy self-sufficiency and the internal rate of return of the investment. Time series from a real data centre were used for the annual simulations.

The optimisation variables concerned both the capacity of the PV + CB system, and the thermodynamic cycle of the CB. A parametric analysis was also used to study the case where the investment cost for the CB would be halved. Finally, the designs giving rise to high self-sufficiency ratios were analysed in more details.

Based on the results obtained, the following conclusions can be drawn:

- Despite its low efficiency (i.e. $< 30\%$) and high investment cost (i.e. > 6500 €/kW, $>$ 580 €/kWh), the CB is necessary for increasing the SSR above 40%. Below this level, PV alone is preferable. This threshold is close to the maximum SSR obtainable with PV alone, but it remains specific to the considered economic model. Hence, it may vary according to the costs chosen: for instance, lower investment costs for the CB or higher electricity prices would reduce it.

  It should also be noted that, although the storage efficiency is lower in Seville than in Louvain-la-Neuve, the CB + PV system is more profitable there thanks to the higher solar irradiance (i.e. 50% more).

  It is also possible to think that, from a strictly techno-economic point of view, chemical batteries are likely to perform better than the CB, due to their much higher efficiency (usually $> 90\%$) and lower cost. However, a more relevant comparison between these two technologies would seem to be the environmental impact, given that the Carnot battery is, in principle, more sparing of rare materials. This point deserves more in-depth LCA studies, and should be investigated in future works.

- Once the maximum PV capacity has been installed, the SSR can still be slightly increased. This is done by increasing the storage capacity above its economically optimal value. The nominal discharge time is then increased from a daily value (i.e. approximately 12 h) to a higher value, which exponentially increases the costs.

- When the heat source of the Carnot battery is at low temperature (e.g. scenarios A and C), it is financially more attractive to use resistive heating to charge the system. On the other hand, when the aim is to maximise the SSR, the use of a heat pump becomes necessary in order to increase the efficiency of the Carnot battery. However, when the amount of thermal energy available at the source is limited (e.g. scenario A), the use of a booster is essential to increase the charging capacity. Yet, using this booster reduces the COP. There is therefore a dilemma between efficiency and charging capacity.

  When the heat source is at a higher temperature (e.g. scenario B), the heat pump is the most financially attractive option. But when aim is to increase the SSR, the booster dilemma still applies.

- The fraction of waste heat recovered by the HP does not exceed 40% in the best case. To increase this, the charging period would have to be increased. This could be achieved by using another renewable source, such as wind power. Also, placing the PV in different orientations would make it possible to spread out the production peak.

- Considering the observations made in this study, it is recommended that future works further investigate the booster dilemma, which is defined as the conflict between the COP and the charging capacity in thermally integrated heat pumps. This dilemma was introduced here with the case of Carnot batteries, but could also be encountered in other applications, such as waste heat recovery high temperature heat pumps.

  In this work, resistive heating was considered as booster. However, more efficient configurations must be studied to alleviate the intensity of this dilemma. Dual heat source heat pumps are an option that should be explored.

- Conservative costs and performance values were used in this work. However, there is still room for improvement. Indeed, in addition to dual heat source heat pumps, there are margins for efficiency gains, and these should be considered in future works. For instance, the isentropic efficiency of the compression and expansion machines could be increased, using turbomachines. The constraints on the flexibility and part load operations should then be considered. Also, to reduce compression ratios, multi-stage cycles could be considered.

It has also been shown that halving the investment costs in the CB can halve the payback period for an equivalent SSR. Reducing the capital costs should therefore be a priority for future works in this field, so as to enable the technology to be deployed. A way of achieving that could be the integrated conception of the HP, TES and ORC as a CB (i.e. as opposed to simply juxtaposing them), for example by using reversible HP/ORC [59]. The use of thermal storage in a single stratified tank is also an option to reduce these costs, although it may cause efficiency degradation.

- In this model, only load-shifting of the PV production is considered for the Carnot battery. However, given its relatively poor financial performance, it seems essential to find additional revenue streams. The potential for energy arbitrage could, for instance, be assessed with optimal power flow models. The added value of grid services could also be considered, after a characterisation of the dynamic performance.

Declaration of competing interest

The authors declare that they have no known competing financial interests or personal relationships that could have appeared to influence the work reported in this paper.

Acknowledgements

The first author acknowledges the support of Fonds de la Recherche Scientifique - FNRS [40014566 FRIA-B1].

Computational resources have been provided by the Consortium des Équipements de Calcul Intensif (CÉCI), funded by the Fonds de la Recherche Scientifique de Belgique (F.R.S.-FNRS) under Grant No. 2.5020.11 and by the Walloon Region.

Annual data corresponding to the data centre have been gratefully provided by the Center for High Performance Computing and Mass Storage (CISM) from UCLouvain.

References

[1] A. V. Olympios, J. D. McTigue, P. Farres-Antunez, A. Tafone, A. Romagnoli, Y. Li, Y. Ding, W.-D. Steinmann, L. Wang, H. Chen, C. N. Markides, Progress and prospects of thermo-mechanical energy storage—a critical review, Progress in Energy 3 (2) (2021) 022001. doi:10.1088/2516-1083/abdbba.
URL https://iopscience.iop.org/article/10.1088/2516-1083/abdbba

[2] J. Ramsebner, R. Haas, A. Ajanovic, M. Wietschel, The sector coupling concept: A critical review, Wiley Interdisciplinary Reviews: Energy and Environment 10 (4) (2021) e396, publisher: Wiley Online Library.

[3] W.-D. Steinmann, D. Bauer, H. Jockenhöfer, M. Johnson, Pumped thermal energy storage (PTES) as smart sector-coupling technology for heat and electricity, Energy 183 (2019) 185–190. doi:10.1016/j.energy.2019.06.058.
URL http://www.sciencedirect.com/science/article/pii/S0360544219311879

[4] G. F. Frate, M. Antonelli, U. Desideri, A novel Pumped Thermal Electricity Storage (PTES) system with thermal integration, Applied Thermal Engineering 121 (2017) 1051–1058. doi:10.1016/j.applthermaleng.2017.04.127.
URL https://linkinghub.elsevier.com/retrieve/pii/S135943111634114X

[5] M. Weitzer, D. Müller, D. Steger, A. Charalampidis, S. Karellas, J. Karl, Organic flash cycles in Rankine-based Carnot batteries with large storage temperature spreads, Energy Conversion and Management 255 (2022) 115323. doi:10.1016/j.enconman.2022.115323.
URL https://www.sciencedirect.com/science/article/pii/S0196890422001194

[6] O. Dumont, G. F. Frate, A. Pillai, S. Lecompte, M. De Paepe, V. Lemort, Carnot battery technology: A state-of-the-art review, The Journal of Energy Storage 32 (Sep. 2020). doi:10.1016/j.est.2020.101756.

[7] G. F. Frate, L. Ferrari, U. Desideri, Rankine Carnot Batteries with the Integration of Thermal Energy Sources: A Review, Energies 13 (18) (2020) 4766, number: 18 Publisher: Multidisciplinary Digital Publishing Institute. doi:10.3390/en13184766.
URL https://www.mdpi.com/1996-1073/13/18/4766

[8] V. Novotny, V. Basta, P. Smola, J. Spale, Review of Carnot Battery Technology Commercial Development, Energies 15 (2) (2022) 647. doi:10.3390/en15020647.
URL https://www.mdpi.com/1996-1073/15/2/647

[9] H. Jockenhöfer, W.-D. Steinmann, D. Bauer, Detailed numerical investigation of a pumped thermal energy storage with low temperature heat integration, Energy 145 (2018) 665–676. doi:10.1016/j.energy.2017.12.087.
URL https://linkinghub.elsevier.com/retrieve/pii/S0360544217321308

[10] O. Dumont, V. Lemort, Mapping of performance of pumped thermal energy storage (Carnot battery) using waste heat recovery, Energy 211 (2020) 118963. doi:10.1016/j.energy.2020.118963.
URL https://linkinghub.elsevier.com/retrieve/pii/S0360544220320703

[11] S. Staub, P. Bazan, K. Braimakis, D. Müller, C. Regensburger, D. Scharrer, B. Schmitt, D. Steger, R. German, S. Karellas, M. Pruckner, E. Schlücker, S. Will, J. Karl, Reversible Heat Pump–Organic Rankine Cycle Systems for the Storage of Renewable Electricity, Energies 11 (6) (2018) 1352, number: 6 Publisher: Multidisciplinary Digital Publishing Institute. doi:10.3390/en11061352.
URL https://www.mdpi.com/1996-1073/11/6/1352

[12] G. F. Frate, L. Ferrari, U. Desideri, Multi-criteria investigation of a pumped thermal electricity storage (PTES) system with thermal integration and sensible heat storage, Energy Conversion and Management 208 (2020) 112530. doi:10.1016/j.enconman.2020.112530.
URL https://linkinghub.elsevier.com/retrieve/pii/S0196890420300662

[13] M. Weitzer, D. Müller, J. Karl, Two-phase expansion processes in heat pump – ORC systems (Carnot batteries) with volumetric machines for enhanced off-design efficiency, Renewable Energy 199 (2022) 720–732. doi:10.1016/j.renene.2022.08.143.
URL https://www.sciencedirect.com/science/article/pii/S0960148122013222

[14] P. Lu, X. Luo, J. Wang, J. Chen, Y. Liang, Z. Yang, J. He, C. Wang, Y. Chen, Thermodynamic analysis and evaluation of a novel composition adjustable Carnot battery under variable operating scenarios, Energy Conversion and Management 269 (2022) 116117. doi:10.1016/j.enconman.2022.116117.
URL https://www.sciencedirect.com/science/article/pii/S0196890422009013

[15] M. Zhang, L. Shi, P. Hu, G. Pei, G. Shu, Carnot battery system integrated with low-grade waste heat recovery: Toward high energy storage efficiency, Journal of Energy Storage 57 (2023) 106234. doi:10.1016/j.est.2022.106234.
URL https://www.sciencedirect.com/science/article/pii/S2352152X2202223X

[16] A. Vecchi, K. Knobloch, T. Liang, H. Kildahl, A. Sciacovelli, K. Engelbrecht, Y. Li, Y. Ding, Carnot Battery development: A review on system performance, applications and commercial state-of-the-art, Journal of Energy Storage 55 (2022) 105782. doi:10.1016/j.est.2022.105782.
URL https://www.sciencedirect.com/science/article/pii/S2352152X22017704

[17] G. F. Frate, L. Ferrari, P. Sdringola, U. Desideri, A. Sciacovelli, Thermally integrated pumped thermal energy storage for multi-energy districts: Integrated modelling, assessment and comparison with batteries, Journal of Energy Storage 61 (2023) 106734. doi:10.1016/j.est.2023.106734.
URL https://www.sciencedirect.com/science/article/pii/S2352152X23001317

[18] S. Hu, Z. Yang, J. Li, Y. Duan, Thermo-economic analysis of the pumped thermal energy storage with thermal integration in different application scenarios, Energy Conversion and Management 236 (2021) 114072. doi:10.1016/j.enconman.2021.114072.
URL https://linkinghub.elsevier.com/retrieve/pii/S019689042100248X

[19] R. Fan, H. Xi, Energy, exergy, economic (3E) analysis, optimization and comparison of different Carnot battery systems for energy storage, Energy Conversion and Management 252 (2022) 115037. doi:10.1016/j.enconman.2021.115037.
URL https://www.sciencedirect.com/science/article/pii/S0196890421012139

[20] K. Ökten, B. Kurşun, Thermo-economic assessment of a thermally integrated pumped thermal energy storage (TI-PTES) system combined with an absorption refrigeration cycle driven by low-grade heat source, Journal of Energy Storage 51 (2022) 104486. doi:10.1016/j.est.2022.104486.
URL https://www.sciencedirect.com/science/article/pii/S2352152X22005084

[21] Y. Zhang, L. Xu, J. Li, L. Zhang, Z. Yuan, Technical and economic evaluation, comparison and optimization of a Carnot battery with two different layouts, Journal of Energy Storage 55 (2022) 105583. doi:10.1016/j.est.2022.105583.
URL https://www.sciencedirect.com/science/article/pii/S2352152X22015717

[22] G. F. Frate, L. Ferrari, U. Desideri, Multi-Criteria Economic Analysis of a Pumped Thermal Electricity Storage (PTES) With Thermal Integration, Frontiers in Energy Research 8 (2020) 53. doi:10.3389/fenrg.2020.00053.
URL https://www.frontiersin.org/article/10.3389/fenrg.2020.00053/full

[23] P. Sorknæs, J. Z. Thellufsen, K. Knobloch, K. Engelbrecht, M. Yuan, Economic potentials of carnot batteries in 100% renewable energy systems, Energy 282 (2023) 128837. doi:10.1016/j.energy.2023.128837.
URL https://www.sciencedirect.com/science/article/pii/S0360544223022314

[24] H. Lund, J. Z. Thellufsen, P. A. Østergaard, P. Sorknæs, I. R. Skov, B. V. Mathiesen, EnergyPLAN – Advanced analysis of smart energy systems, Smart Energy 1 (2021) 100007. doi:10.1016/j.segy.2021.100007.
URL https://www.sciencedirect.com/science/article/pii/S2666955221000071

[25] R. Tassenoy, K. Couvreur, W. Beyne, M. De Paepe, S. Lecompte, Techno-economic

assessment of Carnot batteries for load-shifting of solar PV production of an office building, Renewable Energy 199 (2022) 1133–1144. doi:10.1016/j.renene.2022.09.039.
URL https://www.sciencedirect.com/science/article/pii/S0960148122013891

[26] C. Poletto, A. De Pascale, S. Ottaviano, O. Dumont, A. Alessandra Maria, M. Bianchi, Performance and economic assessment of a thermally integrated reversible HP/ORC Carnot battery applied to data centers, in: Proceedings of the 7th International Seminar on ORC Power Systems 2023, Seville, 2023.

[27] J. D. McTigue, P. Farres-Antunez, K. S. J, C. N. Markides, A. J. White, Techno-economic analysis of recuperated Joule-Brayton pumped thermal energy storage, Energy Conversion and Management 252 (2022) 115016. doi:10.1016/j.enconman.2021.115016.
URL https://www.sciencedirect.com/science/article/pii/S0196890421011924

[28] K. Ebrahimi, G. F. Jones, A. S. Fleischer, A review of data center cooling technology, operating conditions and the corresponding low-grade waste heat recovery opportunities, Renewable and Sustainable Energy Reviews 31 (2014) 622–638. doi:10.1016/j.rser.2013.12.007.
URL https://www.sciencedirect.com/science/article/pii/S1364032113008216

[29] S. Pfenninger, I. Staffell, Long-term patterns of European PV output using 30 years of validated hourly reanalysis and satellite data, Energy 114 (2016) 1251–1265. doi:10.1016/j.energy.2016.08.060.
URL https://www.sciencedirect.com/science/article/pii/S0360544216311744

[30] I. Staffell, S. Pfenninger, Using bias-corrected reanalysis to simulate current and future wind power output, Energy 114 (2016) 1224–1239. doi:10.1016/j.energy.2016.08.068.
URL https://www.sciencedirect.com/science/article/pii/S0360544216311811

[31] G. F. Frate, A. Baccioli, L. Bernardini, L. Ferrari, Assessment of the off-design performance of a solar thermally-integrated pumped-thermal energy storage, Renewable Energy 201 (2022) 636–650. doi:10.1016/j.renene.2022.10.097.
URL https://www.sciencedirect.com/science/article/pii/S0960148122015993

[32] I. H. Bell, J. Wronski, S. Quoilin, V. Lemort, Pure and pseudo-pure fluid thermophysical property evaluation and the open-source thermophysical property library CoolProp, Industrial & engineering chemistry research 53 (6) (2014) 2498–2508, publisher: ACS Publications.

[33] M. Pitarch I Mocholí, High capacity heat pump development for sanitary hot water production, Ph.D. thesis, Universitat Politècnica de València, Valencia (Spain), university: Universitat Politècnica de València (Apr. 2017). doi:10.4995/Thesis/10251/81858.
URL https://riunet.upv.es/handle/10251/81858

[34] K.-K. Cao, A. N. Nitto, E. Sperber, A. Thess, Expanding the horizons of power-to-heat: Cost assessment for new space heating concepts with Wind Powered Thermal Energy Systems, Energy 164 (2018) 925–936. doi:10.1016/j.energy.2018.08.173.
URL https://www.sciencedirect.com/science/article/pii/S0360544218317092

[35] D. Maraver, J. Royo, V. Lemort, S. Quoilin, Systematic optimization of subcritical and transcritical organic Rankine cycles (ORCs) constrained by technical parameters in multiple applications, Applied Energy 117 (2014) 11–29. doi:10.1016/j.apenergy.2013.11.076.
URL https://www.sciencedirect.com/science/article/pii/S0306261913009859

[36] A. Laterre, O. Dumont, V. Lemort, F. Contino, Systematic and multi-criteria optimisation of subcritical thermally integrated Carnot batteries (TI-PTES) in an extended domain, in: Proceedings of the 7th International Seminar on ORC Power Systems 2023, Seville, 2023.

[37] A. H. Hassan, J. M. Corberán, M. Ramirez, F. Trebilcock-Kelly, J. Payá, A high-

temperature heat pump for compressed heat energy storage applications: Design, modeling, and performance, Energy Reports 8 (2022) 10833–10848. doi:10.1016/j.egyr.2022.08.201.
URL https://www.sciencedirect.com/science/article/pii/S2352484722016456

[38] W. F. Holmgren, C. W. Hansen, M. A. Mikofski, pvlib python: a python package for modeling solar energy systems, Journal of Open Source Software 3 (29) (2018) 884. doi:10.21105/joss.00884.
URL https://joss.theoj.org/papers/10.21105/joss.00884

[39] D. Coppitters, W. De Paepe, F. Contino, Robust design optimization and stochastic performance analysis of a grid-connected photovoltaic system with battery storage and hydrogen storage, Energy 213 (2020) 118798. doi:10.1016/j.energy.2020.118798.
URL https://linkinghub.elsevier.com/retrieve/pii/S0360544220319058

[40] W. De Soto, S. A. Klein, W. A. Beckman, Improvement and validation of a model for photovoltaic array performance, Solar Energy 80 (1) (2006) 78–88. doi:10.1016/j.solener.2005.06.010.
URL https://www.sciencedirect.com/science/article/pii/S0038092X05002410

[41] SUNPOWER, X-SERIES RESIDENTIAL SOLAR PANELS: SUPPLEMENTARY TECHNICAL SPECIFICATIONS.

[42] G. A. Rampinelli, A. Krenzinger, F. Chenlo Romero, Mathematical models for efficiency of inverters used in grid connected photovoltaic systems, Renewable and Sustainable Energy Reviews 34 (2014) 578–587. doi:10.1016/j.rser.2014.03.047.
URL https://www.sciencedirect.com/science/article/pii/S1364032114002081

[43] T.-S. Lee, Second-Law Analysis to Improve the Energy Efficiency of Screw Liquid Chillers, Entropy 12 (3) (2010) 375–389, number: 3 Publisher: Molecular Diversity Preservation International. doi:10.3390/e12030375.
URL https://www.mdpi.com/1099-4300/12/3/375

[44] M. Montero Carrero, Decoupling heat and electricity production from micro gas turbines: numerical, experimental and economic analysis of the micro humid air turbine cycle, Ph.D. thesis, Vrije Universiteit Brussel (Jun. 2018).
URL http://hdl.handle.net/2013/

[45] Eurostat, Electricity prices for non-household consumers - bi-annual data (from 2007 onwards) (Apr. 2022).

[46] A. Laterre, O. Dumont, V. Lemort, F. Contino, Design Optimisation and Global Sensitivity Analysis of a Carnot Battery Towards Integration in a Data Centre under Techno-Economic Uncertainties, in: Proceedings of 5th SEE SDEWES, Vlorë, Albania, 2022, p. 19.

[47] D. Coppitters, K. Verleysen, W. De Paepe, F. Contino, How can renewable hydrogen compete with diesel in public transport? Robust design optimization of a hydrogen refueling station under techno-economic and environmental uncertainty, Applied Energy 312 (2022) 118694. doi:10.1016/j.apenergy.2022.118694.
URL https://www.sciencedirect.com/science/article/pii/S0306261922001581

[48] D. E. Agency, Technology Data for Generation of Electricity and District Heating, Tech. rep., Danish Energy Agency (Feb. 2023).

[49] C. Arpagaus, F. Bless, M. Uhlmann, J. Schiffmann, S. S. Bertsch, High temperature heat pumps: Market overview, state of the art, research status, refrigerants, and application potentials, Energy 152 (2018) 985–1010. doi:10.1016/j.energy.2018.03.166.
URL https://www.sciencedirect.com/science/article/pii/S0360544218305759

[50] S. Meyers, B. Schmitt, K. Vajen, The future of low carbon industrial process heat: A comparison between solar thermal and heat pumps, Solar Energy 173 (2018) 893–904. doi:10.1016/j.solener.2018.08.011.
URL https://www.sciencedirect.com/science/article/pii/S0038092X18307801

[51] M. Shamoushaki, P. H. Niknam, L. Talluri, G. Manfrida, D. Fiaschi, Development of Cost Correlations for the Economic Assessment of Power Plant Equipment, Energies 14 (9) (2021) 2665. doi:10.3390/en14092665.
URL https://www.mdpi.com/1996-1073/14/9/2665

[52] S. Quoilin, S. Declaye, B. F. Tchanche, V. Lemort, Thermo-economic optimization of waste heat recovery Organic Rankine Cycles, Applied Thermal Engineering 31 (14) (2011) 2885–2893. doi:10.1016/j.applthermaleng.2011.05.014.
URL https://www.sciencedirect.com/science/article/pii/S1359431111002663

[53] D. Coppitters, P. Tsirikoglou, W. D. Paepe, K. Kyprianidis, A. Kalfas, F. Contino, RHEIA: Robust design optimization of renewable Hydrogen and dErIved energy cArrier systems, Journal of Open Source Software 7 (75) (2022) 4370. doi:10.21105/joss.04370.
URL https://joss.theoj.org/papers/10.21105/joss.04370

[54] S. Lemmens, Cost Engineering Techniques and Their Applicability for Cost Estimation of Organic Rankine Cycle Systems, Energies 9 (7) (2016) 485. doi:10.3390/en9070485.
URL http://www.mdpi.com/1996-1073/9/7/485

[55] K. Deb, A. Pratap, S. Agarwal, T. Meyarivan, A fast and elitist multiobjective genetic algorithm: NSGA-II, IEEE transactions on evolutionary computation 6 (2) (2002) 182–197, publisher: IEEE.

[56] D. Coppitters, W. De Paepe, F. Contino, Robust design optimization of a photovoltaic-battery-heat pump system with thermal storage under aleatory and epistemic uncertainty, Energy 229 (2021) 120692. doi:10.1016/j.energy.2021.120692.
URL https://linkinghub.elsevier.com/retrieve/pii/S0360544221009403

[57] M. I. Hlal, V. K. Ramachandaramurthya, S. Padmanaban, H. R. Kaboli, A. Pouryekta, T. A. R. b. T. Abdullah, NSGA-II and MOPSO based optimization for sizing of hybrid PV/wind/battery energy storage system, International Journal of Power Electronics and

Drive Systems (IJPEDS) 10 (1) (2019) 463–478, number: 1. doi:10.11591/ijpeds.v10.i1.pp463-478.
URL https://ijpeds.iaescore.com/index.php/IJPEDS/article/view/14754

[58] Lithium-ion Battery Pack Prices Rise for First Time to an Average of $151/kWh, section: Press Release (Dec. 2022).
URL https://about.bnef.com/blog/lithium-ion-battery-pack-prices-rise-for-first-time

[59] O. Dumont, S. Quoilin, V. Lemort, Experimental investigation of a reversible heat pump/organic Rankine cycle unit designed to be coupled with a passive house to get a Net Zero Energy Building, International Journal of Refrigeration 54 (2015) 190–203. doi:10.1016/j.ijrefrig.2015.03.008.
URL https://linkinghub.elsevier.com/retrieve/pii/S0140700715000638